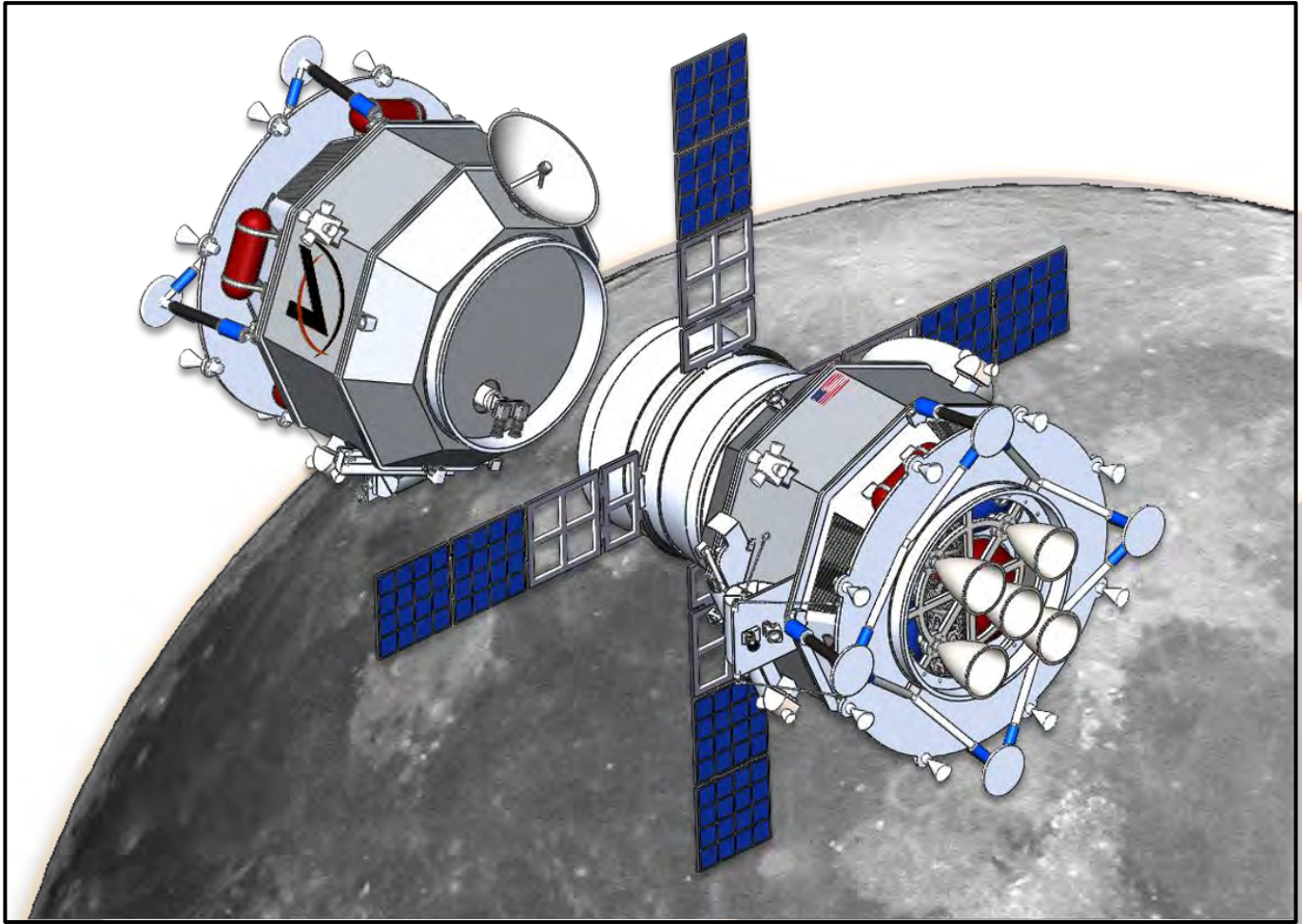


AIAA 2018 Undergraduate Spacecraft Design Competition



Project DIANA:
*Dual Lunar Ice Analyzers Supporting
Next-Gen Astronautics*

Design Proposal by

ASCENSION INDUSTRIES

California Polytechnic State University, Pomona



ASCENSION INDUSTRIES



Will Morris
Team Lead
AIAA Member # 920006



Dr. Donald Edberg
Team Advisor
AIAA Member # 22972



Max Feagle
Deputy Team Lead
AIAA Member # 922677



Thomas Fergus
Lead Guidance Engineer
AIAA Member # 920792



Samuel Kim
Lead Structural Engineer
AIAA Member # 922679



Marco Filecchia
Lead Component Designer
AIAA Member # 922643



Josh Kennedy
Lead Thermal Analyst
AIAA Member # 922673



Damian Magaña
Lead Propulsion Engineer
AIAA Member # 922683





Extended Executive Summary

Lunar water is instrumental for colonization of the Earth’s nearest celestial neighbor. Due to its weight, it would be economically infeasible to lift significant quantities of this essential resource into Earth orbit and beyond. A lunar colony becomes a much more feasible endeavor if there exist resources on the Moon that can be utilized in-situ. Missions such as NASA’s Lunar Reconnaissance Orbiter (LRO) and India’s Chandrayaan-1 have provided enticing evidence of lunar water ice present in the lunar poles. The objective of Project DIANA is to seek out potential locations of this valuable resource, confirm its existence, and to do so cost-effectively, under budget and within schedule. This mission’s success would provide a crucial stepping stone in the ultimate goal of establishing a Martian colony.

The driving requirements for our mission design included the accurate quantification of water in two different lunar craters, overall mission cost under \$500 M (FY17), maximized science return, and mission completion by the end of 2024. These driving requirements are discussed in more detail in **Section 1.1**. A complete compliance matrix can be found in **Section 5.5**. A brief compliance matrix of key mission requirements is present at the end of this summary.

Two different architectures were considered to meet these mission objectives: one “conventional” and one “inventive”. The conventional architecture was comprised of two identical landers, which would provide a reliable, tried and true design, but with limited scientific return. On the other hand, the inventive architecture utilized a novel concept featuring an orbiter with science payload impactors which would search for water using seismic activity. This trade study is discussed in detail in **Section 1.2**. We decided on the conventional architecture due to the reliability inherent in a lander-type design and its overall lower cost (\$448 M for conventional design vs \$812 M for the inventive design). The down-select lander architecture is shown below in Figure EXEC-1.

Coupled (DI+II) Configuration

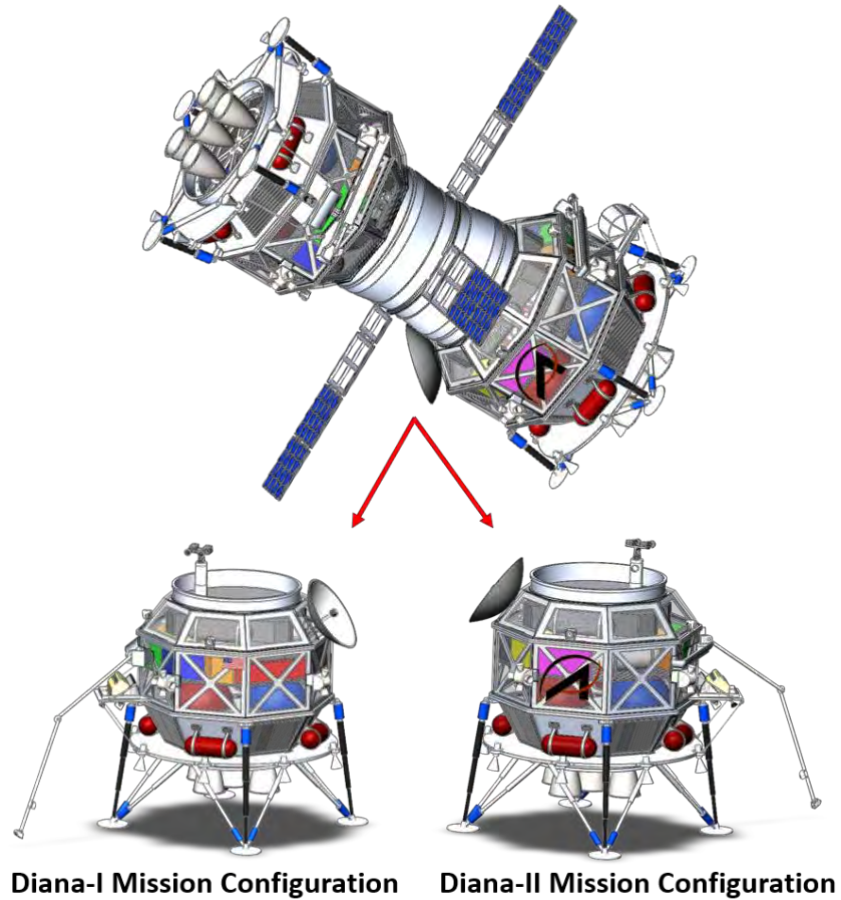


Figure EXEC-1: Dual Lander Spacecraft, Coupled and Mission Configurations

The design consists of a dual-lander system capable of landing softly in two different permanently shadowed lunar craters. The landers are joined together with an interfacing coupler, which is comprised of off the shelf components (RUAG[®] launch vehicle adapters and separation rings). The coupler also houses the solar panels that power the spacecraft during the transit time to the Moon. The coupler is designed to be discarded at spacecraft separation so that the solar panels do not hinder surface operations, as they are no longer needed in the permanently shadowed craters targeted. The spacecraft is designed using a tiered system and an octagonal frame that makes production easier as well as provide greater structural integrity; a complete stress analysis can be found in **Section 4.8.2**. The primary payload instruments consist of a Robotic Arm and a Sample Analyzer with mass spectrometer for quantification of water and other volatiles directly from samples of regolith. Payload instruments are described in depth in **Section 2.3**.



Landing site selection was performed by selecting craters which have previously established indications of water ice and can provide clear line of sight for direct to Earth communications. The selected landing site locations which best met these criteria are craters *Scott* and *Nobile* located near the lunar southern pole. These craters are identified in Figure EXEC-2. More details regarding landing site selection and communications architecture design can be found in **Section 2.2**.

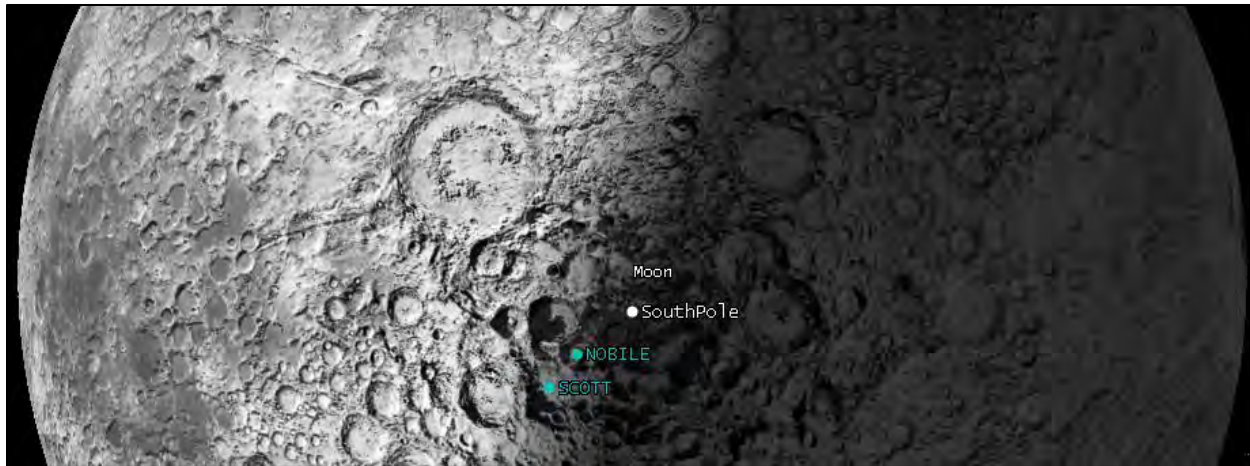


Figure EXEC-2: Landing Sites Relative to South Pole

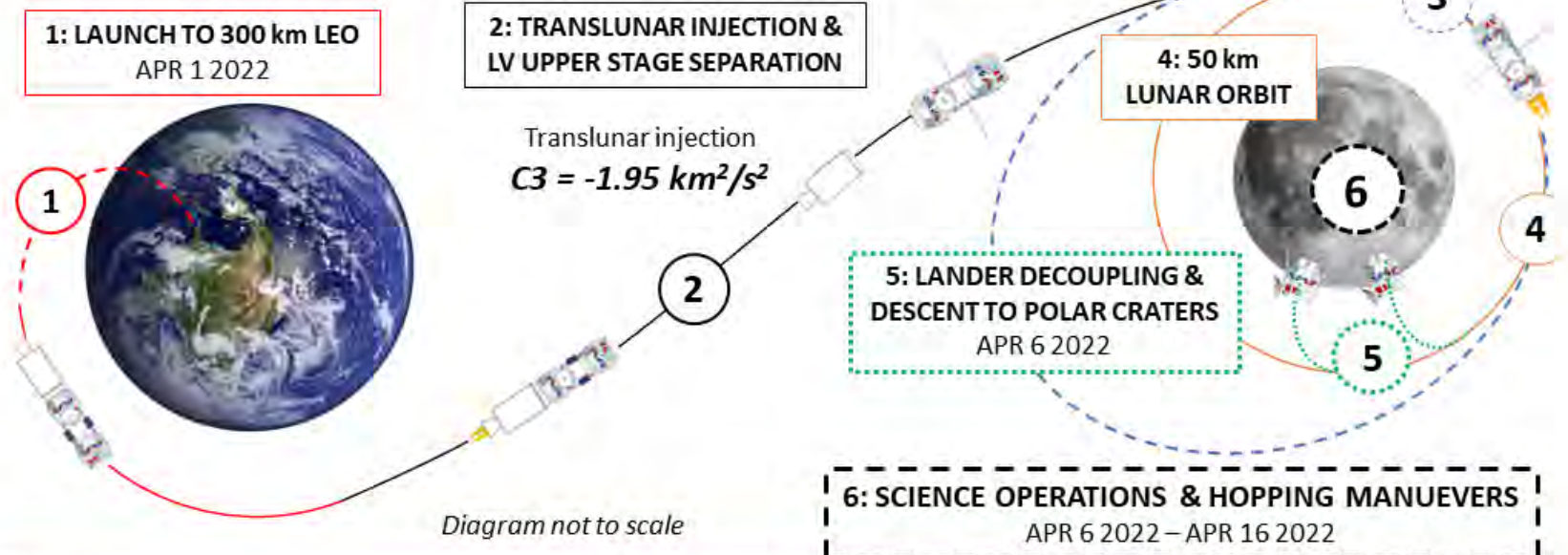
DIANA will launch April 1st, 2022 into Low Earth Orbit (LEO) followed by a coast phase of about 45 minutes. Then the Falcon 9 second stage engine will reignite, placing the landers on a ballistic trajectory to the moon. On lunar approach, the landers will perform two maneuvers that capture the mission into lunar orbit. The first maneuver places DIANA into an ellipse with periapsis altitude of 50 km. The second circularizes the orbit at a constant altitude of 50 km. A concept of operations overview is shown below in Figure EXEC-3. A complete detailed breakdown of the trajectory design is presented in **Section 3.3**.

The landers are equipped with extra fuel and Vernier engines to “hop” to a different location (as described in section 3.4) after sample collection and analysis is complete in the initial landing spot, allowing it to collect samples from multiple locations and thereby providing more robust scientific return. More detail about this can be found in **Section 3.4**, Landing and Hopping Detail and **Section 3.5**, Science Operations.



Project DIANA

Concept of Operations Overview



CONOPS Stage	Description	ΔV (km/s)	Provided By
1	Launch to 300 km LEO	9.30	Falcon 9 FT
2	Translunar Injection (TLI)	3.11	Falcon 9 FT Upper Stage
3-B1	Lunar Capture Burn #1	0.39	Diana I
3-B2	Lunar Capture Burn #2	0.43	Diana II
4	50 km Polar Lunar Orbit	-	-
5-L1	Diana I Decoupling, Descent, and Landing in Crater <i>Nobile</i>	1.85	Diana I
5-IC	Diana II Inclination Change	0.07	Diana II
5-L2	Diana II Decoupling, Descent, and Landing in Crater <i>Scott</i>	1.85	Diana II
6	Science Mission	-	-

Figure EXEC-3: CONOPS Overview



Within the craters, DIANA-I and II will link direct line of sight to either White Sands Ground Station or Wallops Island. The spacecraft can link at a rate of 20 Mbps to either station with sufficient data link margin. At this data rate it will need to link for 1 hour every day during our science mission to avoid filling the solid-state drives to capacity. Fortunately, DIANA has a 12-hour window every day during the duration of our science mission. This is elaborated on **Section 2.2**, Landing Site Selection, and **4.6**, Telecommunication.

The propulsion system's design is driven by the requirements for ΔV , restart and throttle capabilities, and water contamination risks. To down-select candidates for the design, trade studies were first conducted on the types of propulsion systems available, followed by trade studies on the propellants and engines to be used. A further discussion on these trade studies can be found in **Section 4.2**.

The landers make use of a fuel cell system to provide power in the craters. The fuel cells will also provide power during the peak power draws for the engine burns. The system is sized for 15 days of continuous operation at 656 Watts. This gives the landers 5 days of power margin since the science mission is expected to last 10 days. During the initial launch and cruise phases the landers receive power from solar panels and LiPo batteries these systems can also provide power in the event of a mission pause such as having to stay in LEO longer than expected due to a failure at checkout. The full details can be found in **Section 4.3**.

The thermal protection system (TPS) consists of a passive system using MLI to maintain the internal temperature of the landers. Louvers, heat pipes, and radiators are also used to maintain thermal equilibrium. Additional, two heaters are used in the event of a failure in the passive system to keep the landers warm in the craters. Using MLI posed heating challenges during the flight, but the transient analysis showed the TPS can handle all of the temperature regimes. Full details can be found in **Section 4.4**.

The attitude control system (ACS) consists of 12 coupled thrusters for maneuvering and orienting and a rich set of ancillary equipment. A full, detailed description of each, including trade studies can be found in **4.5**.

To keep the landers able to be commanded, as well as capable of onboard data management and storage each lander is equipped with a command and data system, which is discussed in more in **4.7**.

Structural analysis was performed with the aid of computer programs such as SOLIDWORKS Simulation which simplifies the tasks of the structural analyst and create short work of otherwise long hand calculation. Finite



element analysis for the spacecraft's structure can be seen in **Section 4.8.2** while analysis of the landing leg can be found in **Section 4.8.3**. Necessary mechanisms are discussed in **Section 4.8.4**.

Cost estimation was performed using the NASA Instrument Cost Model (NICM) as well as the USAF Unmanned Spacecraft Cost Model (USCM8). Payload instrument cost was first estimated using NICM, and then the spacecraft bus components and well as programmatic costs such as Integration, Assembly, and Testing were estimated using USCM8. Program schedule is presented in **Section 5.1**. A work breakdown structure of cost elements is presented in **Section 5.3** and an in-depth discussion on cost estimation can be seen in **Section 5.4**. Complete cost estimate breakdowns can be found in Appendix A. A brief compliance matrix of driving requirements is shown below in Table EXEC-1.

Exhaustive effort has been spent on this proposal in the aim of thoroughly satisfying all requirements and mission prerequisites. It is our hope that this effort is clearly evidenced throughout the submission, and we thank the review board for taking the time to review it.

Table EXEC-1: Compliance Matrix of Driving Requirements

Rq. #	Requirement Text	Met?	Explanation
00.0.001	Mission shall determine the locations and quantities of water deposits in terms of the ratio of water to regolith in two lunar craters.	Yes	Dual lander architecture allows for the exploration of two lunar craters. Robotic Arm & SAMZER allow for in situ measurements of regolith in terms of water composition.
00.0.004	Mission shall describe the experiment operations and communication plans.	Yes	Landers' Fuel Cells allow 10 days of continuous operation, with the S-Band HGA capable of downlink to Ground.
00.0.006	Mission and design trade studies shall be weighted to prioritize using tech. that have already demonstrated on previous missions or are otherwise in the NASA technology development portfolio and are to be assessed on the basis of benefit, risk and cost	Yes	All instruments are based off historical missions to minimize cost, complexity and were down-selected based on their capability to effectively determine the presence of ice within the lunar environment.
00.1.003	Mission shall maximize scientific data return before the end of the mission date of December 31, 2024.	Yes	Landing targets are permanently shadowed craters (where likelihood of water ice presence is highest), and the landers also can "hop" to nearby areas.
00.2.001	Mission architecture and vehicle design shall maximize science data return within cost of \$500 million United States Dollars in FY 2017	Yes	NICM+USCM8 cost estimation method puts total cost under budget.



Table of Contents

Extended Executive Summary.....	iii
List of Acronyms and Units.....	x
List of Figures.....	xii
List of Tables.....	xiv
1 Mission Overview.....	1
1.1 Driving Requirements.....	1
1.2 Architecture Trade Study and Selection.....	1
1.3 Spacecraft Overview.....	3
2 Science and Instrumentation.....	6
2.1 Science Overview and Historical Context.....	6
2.2 Landing Site Selection.....	7
2.3 Payload Instrumentation and Trade Studies.....	9
2.4 Traceability to Requirements.....	15
2.5 Instruments Summary.....	16
3 Mission Design.....	17
3.1 Launch Vehicle Trade Study and Selection.....	17
3.2 Mission Operations Timeline.....	18
3.3 Trajectory Design.....	18
3.4 Landing and Hopping Detail.....	21
3.5 CONOPS Stage 5: Science Operations.....	23
3.6 End of Mission.....	24
4 Spacecraft Sub-System Design.....	25
4.1 Configuration and Field of View (FoV) Plots.....	25
4.2 Propulsion.....	28
4.3 Power.....	37
4.4 Thermal.....	45
4.5 Attitude Control System (ACS).....	49
4.6 Telecommunications.....	56
4.7 Command and Data System (CDS).....	59
4.8 Structures.....	61
4.9 Fault Analysis and Redundancy.....	68
5 Mission Management.....	70
5.1 Program Schedule.....	70
5.2 Manufacturing.....	70
5.3 Program Work Breakdown Structure.....	72
5.4 Cost Estimates.....	73
5.5 Complete Compliance Matrix.....	74
6 Summary Tables.....	76
6.1 Spacecraft Mass Statements.....	76
6.2 Spacecraft Power Statement.....	77
Appendix A: Complete Cost Estimate Breakdown.....	78
References.....	80



List of Acronyms and Units

Acronym/Unit	Definition
ACS	Attitude Control System
AGE	Aerospace Ground Equipment
ALHAT	Autonomous Landing/Hazard Avoidance Technology
BDS	Bulk Data Storage
bps	bits per second
C	Coupler
CAD	Computer Aided Design/Drafting/Drawing
CDS	Command and Data System
CEP	Circular Error Probable
cm	centimeters
CMD	Command
ConOps	Concept of Operations
DoD	Depth of Discharge
DSN	Deep Space Network
EOL	End of Life
EOM	End of Mission
EPS	Electrical Power System
F9	Falcon 9 Launch Vehicle
FoV	Field of View
FPGA	Field Programmable Gate Array
FY	Fiscal Year
GaAs	Gallium Arsenide
Gb	Gigabit
GRAIL	Gravity Recovery and Interior Laboratory
HGA	High Gain Antenna
HYD	Hydrazine
IMU	Inertial Measurement Unit
IR	Infrared
K	Kelvin
km	kilometer
KSC	Kennedy Space Center
L	Lander
L-SPEC	Laser SPECTrometer
LEO	Low Earth Orbit
LGA	Low Gain Antenna
LiDAR	Light Detection And Ranging
LOI	Lunar Orbit Insertion
LOOS	Launch Operation & Orbital Support



LRO	Lunar Reconnaissance Orbiter
LV	Launch Vehicle
LUNDI	LUNAr Descent Imager
m	meter
Mbps	Megabits per second
MSL	Mars Science Laboratory
NICM	NASA Instrument Cost Model
NTO	Nitrogen Tetroxide
O-MSPA	Offset Multiple Spacecraft Per Aperture
PCB	Printed Circuit Board
PWR	Power
RA	Robotic Arm
RFP	Request for Proposal
s	seconds
SA	Solar Array
SAMZER	SAMple AnalyZER
SC	Spacecraft
SCLK	Spacecraft Clock
SEIS	Seismometer
SLBM	Submarine Launched Ballistic Missile
SOC	String Out Capability
SRB	Solid Rocket Booster
TB	TeraByte
TBD	To Be Determined
TDRSS	Tracking and Data Relay Satellite System
TLI	Trans-Lunar Injection
TLM	Telemetry
TRL	Technology Readiness Level
USAF	United States Air Force
USCM	Unmanned Space Vehicle Cost Model
V	Volts
WSGS	White Sands Ground Station



List of Figures

Figure 1-1: Dual Lander Spacecraft Overview (Shown with Transparent Insulation)	3
Figure 1-2: Lander Payload Instruments	4
Figure 1-3: Spacecraft Summary Sheet	5
Figure 2-1: Hydrogen Concentration at Lunar Poles (Courtesy of Isaacson, Peter)	6
Figure 2-2: Communications Access for Crater “Nobile”, April-May 2022	8
Figure 2-3: Communications Access for Crater “Scott”, April-May 2022.....	8
Figure 2-4: Areas of Strongest Indicated Water Ice Presence in the Lunar South Pole.....	9
Figure 2-5: Robotic Arm (“RA”) Assembly (Left), Robotic Arm Camera (“RAC”, right).....	10
Figure 2-6: SAMZER Instrument Shown in its Retractable Protective Housing	11
Figure 2-7: MastCam-L With Spotlight.....	12
Figure 2-8: LUNDI Position Under SAMZER	13
Figure 2-9: L-SPEC and Position Under MastCam-L	14
Figure 2-10: Reflectance of Water Relative to Wavelength, with Used Wavelength Marked	14
Figure 3-1: To-Scale Resultant Orbits from Lunar Capture Burns.....	20
Figure 3-2: Lunar Hop Sequence.....	22
Figure 3-3: Illustrated Science Operations Flowchart	23
Figure 4-1: Spacecraft Internal Configuration	25
Figure 4-2: Bus Component FoV Plot.....	26
Figure 4-3: FOV Plots for L-SPEC and MastCam-L Payloads	26
Figure 4-4: Field of View for Lunar Descent Imager	27
Figure 4-5: Robotic Arm Range	27
Figure 4-6: Robotic Arm Maximum Depth Achievable (meters).....	28
Figure 4-7: Aluminum Rolling Diaphragm Example	35
Figure 4-8: Propulsion Subsystem Schematic	36
Figure 4-9: Fuel Cell Types and Operating Parameters	40
Figure 4-10: Power System Line Diagram	42
Figure 4-11: Lunar IR Environment	45



Figure 4-12 Thermal Block Diagram.....	47
Figure 4-13: Transient Heating of Landers in 30-day LEO orbit	47
Figure 4-14: Transient Heating of Landers in Transit	48
Figure 4-15: Transient Heating in Lunar Orbit.....	48
Figure 4-16: Picture of Selected ACS Thruster, the Aerojet MR-111C (Courtesy of Aerojet)	51
Figure 4-17: Aerojet MR-111C’s capability to rotate a lander in a 60 second window	52
Figure 4-18: Aerojet MR-111C’s capability to laterally move a lander in a 2 minute window.....	52
Figure 4-19: Landing Site Access Diagram.....	56
Figure 4-20: White Sands Antenna (NASA Goddard Space Flight Center).....	58
Figure 4-21 Expected Launch Accelerations Given by SpaceX User’s Manual	61
Figure 4-22: Payload Coupler System Composed of RUAG and the C15 Adapter.....	63
Figure 4-23: Simulation Results for Given Load Case – Side View	64
Figure 4-24: Load of 35 kN Lander Leg Analysis Side View	65
Figure 4-25: Buckling Analysis with Resulting Load Factor of 1.5	66
Figure 4-26: Fault Analysis Risk Cube.....	69
Figure 5-1: Program Schedule	70
Figure 5-2: Tiered Lander View	71



List of Tables

Table 1-1: Conventional & Invention Architecture Comparison.....	2
Table 2-1: Properties of the Selected Craters, Scott and Nobile.....	7
Table 2-2: Specifications of RA and RAC Instruments.....	10
Table 2-3: Sample Analyzer (SAMZER) Specifications.....	11
Table 2-4: MastCam-L With Spotlight Detailed Information.....	12
Table 2-5: LUNDI Detailed Information.....	13
Table 2-6: Specifications for the L-SPEC Instrument.....	14
Table 2-7: Traceability of Payload Instrument Selection to RFP Requirement.....	15
Table 2-8: Payload Instrument Mass, Power, and Data Rates Summary.....	16
Table 3-1: Launch Vehicle Comparison.....	17
Table 3-2: CONOPS Stage Detail.....	18
Table 4-1: Propulsion System Driving Requirements.....	28
Table 4-2: Main Engine Trade Study.....	30
Table 4-3: Vernier Thruster Trade Study.....	31
Table 4-4: Propellant and Pressurant Mass Calculation.....	33
Table 4-5: Propellant and Pressurant Mass per Lander.....	34
Table 4-6: Propellant & Pressurant Tank Constants.....	34
Table 4-7: Titanium & COPV Tank Sizing.....	35
Table 4-8: Propulsion Subsystem Mass Statement.....	37
Table 4-9: Propulsion Subsystem Power Statement.....	37
Table 4-10: Power System Driving Requirements.....	37
Table 4-11: Power System Trade Study.....	38
Table 4-12: Fuel Cell Characteristics.....	39
Table 4-13: Power System Specifics.....	41
Table 4-14: Coupler Power System Characterist.....	43
Table 4-15: Lander Subsystem Power Budget.....	44
Table 4-16: Power System Mass Statement.....	44
Table 4-17: Driving Thermal Requirements.....	45



Table 4-18: Thermal Limits.....	45
Table 4-19: Steady State Thermal Properties	46
Table 4-20: Orbiter Thermal Control Statement.....	49
Table 4-21: Attitude Control System Requirements.....	49
Table 4-22: Attitude Control System Down-Select Trade Study.....	50
Table 4-23: Attitude Control Thruster Down-Select Trade Study.....	50
Table 4-24: Torques on Landers from Orbital Disturbances	53
Table 4-25: Summation of all Propellant Mass needed by Mission Phase	53
Table 4-26: Trade Study Down-Select for ACS Star Tracker	54
Table 4-27: Trade Study Down-Select for ACS Sun Sensor	54
Table 4-28: Trade Study Down-Select for ACS Inertial Measurement Unit	55
Table 4-29: ALHAT Performance Characteristics	55
Table 4-30: Attitude Control System Mass and Power Statement.....	56
Table 4-31: Ground Station Link Budgets Important Results	57
Table 4-32: Telecommunications Mass and Power Statement	59
Table 4-33: Estimations of the Payload Instrument’s Average Science Data Rates as Based on Historical Information	59
Table 4-34: Approximation of Total Science Mission Data Volume	60
Table 4-35: Command and Data System Mass and Power Statement ⁹	60
Table 4-36: Aluminum Alloy Trade Study.....	62
Table 4-37: Launch Vehicle Interface and Coupler Structure Specification	63
Table 4-38: Summary of Mechanism Table ⁹	67
Table 4-39: Summary of Fault Analysis.....	68
Table 5-1: DIANA – I and II Payload Estimation	73
Table 5-2: System Cost Compliance Summary	74
Table 5-3: Compliance Matrix of all RFP Requirements with Justification.....	75
Table 6-1: Single Lander Mass Statement.....	76
Table 6-2: Coupler Mass Statement.....	76
Table 6-3: Combined Mass Statement Summary	77
Table 6-4: Spacecraft Power Statement.....	77



1 Mission Overview

1.1 Driving Requirements

For meeting the objectives stated in the RFP, the following requirements were identified as design drivers and were assigned ranks relative to one another:


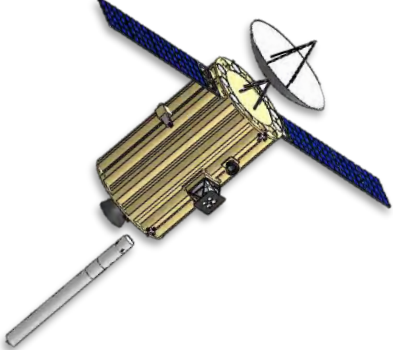
- 1) Determine ratio of water to regolith in two lunar craters (by mass or volume)
- 2) Mission cost below \$500M (FY17 dollars)
- 3) Maximized science data return
- 4) Maximized use of previously demonstrated technologies
- 5) Primary science mission completed by 12/31/2024

1.2 Architecture Trade Study and Selection

Over a period of 3 months, two independent architectures capable of completing the primary mission were designed. The first architecture was a conventional design which consisted of two identical lunar landers that would sample regolith and analyze its volatiles for traces of water. The second was an inventive design that used an orbiter equipped with 8 science impactors that would land on the surface of the moon and use seismic activity to analyze volatiles deep under the lunar surface. These architectures were fully sized, including payload instrument selection, spacecraft subsystem designs, individual concepts of operation, estimation of mission cost, and so forth.

After the independent development of the two architectures crossed their respective systems definition reviews, an architecture down-select trade study was performed. This down-select considered each design's total mission cost, scientific return potential, and operational risk. A summation of this trade study is shown in Table 1-1.

Table 1-1: Conventional & Invention Architecture Comparison

Conventional Architecture: Dual Landers	Inventive Architecture: Science Impactors
	
<p style="text-align: center;"><u>Description:</u></p> <ul style="list-style-type: none"> • 2x identical landers w/ interfacing coupler • “Land and die” concept within two separate permanently shadowed craters • Extracts & analyzes regolith samples directly <p style="text-align: center;"><u>Advantages:</u></p> <ul style="list-style-type: none"> • Solely uses already proven technology • Total mission cost of \$446M (FY17) • Tested and proven approach <p style="text-align: center;"><u>Cons:</u></p> <ul style="list-style-type: none"> • Stationary platform limits scientific return 	<p style="text-align: center;"><u>Description:</u></p> <ul style="list-style-type: none"> • Equipped with 8 Science Impactors • Analyzes volatiles deep under lunar surfaces using seismic activity • Orbiter determines optimal target sites <p style="text-align: center;"><u>Advantages:</u></p> <ul style="list-style-type: none"> • Potentially larger scientific return • Able to sample more than 2 lunar craters <p style="text-align: center;"><u>Cons:</u></p> <ul style="list-style-type: none"> • Estimated to cost \$812M (FY17), well over the \$500M requirement • Novel & unproven operational concept

From this trade study, it was determined that the conventional, lunar lander architecture was superior as its tried and true approach decreases operational risk, its increased use of proven technology lowered mission cost, and its regolith sampling capability allowed for more precise assessment of volatiles. The capabilities of the landers were then expanded following the down-select to mitigate their relative disadvantage of limited scientific return. The propulsion subsystem capability of each lander was increased to allow them to “hop” to 3 additional sites within their respective craters. This increased the overall projected expense to \$493 M, which is still under budget. This addition allows for additional scientific return by having analysis of regolith in several locales, as opposed to a singular one.



1.3 Spacecraft Overview

Our down-selected spacecraft architecture is comprised of two identical landers (DIANA-I and DIANA-II) and an expendable interfacing coupler, shown below in Figure 1-1. The landers travel in a coupled configuration and become fully independent spacecraft following their separation from the coupler immediately before their individual descent burns to the lunar surface. While on the lunar surface, the landers are powered by gaseous oxygen and hydrogen fuel cells. With this design, the landers can draw power from the coupler's solar array during transit without consuming fuel from their fuel cells. Additionally, by ditching the coupler in lunar orbit, propellant savings are achieved since no unnecessary mass is brought to the lunar surface with the landers.

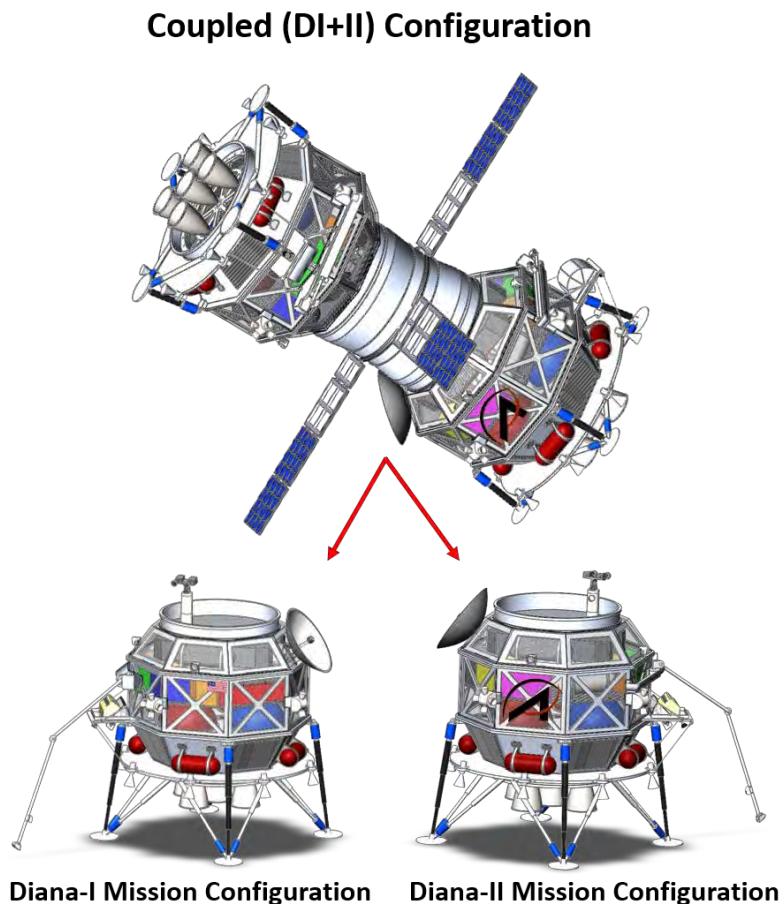


Figure 1-1: Dual Lander Spacecraft Overview (Shown with Transparent Insulation)

Each lander's primary payload consists of a Robotic Arm (RA) and Sample Analyzer (SAMZER), which are both based on counterparts from the Phoenix Mars Lander mission. SAMZER is based on TEGA (Thermal and



Evolved Gas Analyzer) and features a mass spectrometer for accurate quantification of water and other related volatiles such as hydrogen. The Robotic Arm can deposit 16 individual regolith samples into SAMZER for analysis, which is twice the sampling capability of TEGA.

Each lander has been designed with the capability to “hop” to new locations within their respective craters for additional area sampling. The nominal sampling architecture accounts for 4 discrete samples at 4 different landing sites.

Other payload instrumentation included on each lander consists of: a high resolution panoramic camera system (MastCam-L); a laser spectrometer (L-SPEC) for identifying nearby sampling areas of interest; a descent imager (LUNDI); and a Robotic Arm Camera to guide the Robotic Arm’s sample collecting activities. Spotlights were also accounted for to illuminate the lunar surface for imaging. These instruments are shown below in Figure 1-2, are described in detail in 2.3.

Each lander’s sub-systems were thoroughly designed to account for the technical challenges of all mission segments. Fault analysis and risk mitigations were also performed. These analyses can be found throughout Section 4. A dimensioned architecture summary sheet can be seen in Figure 1-3.

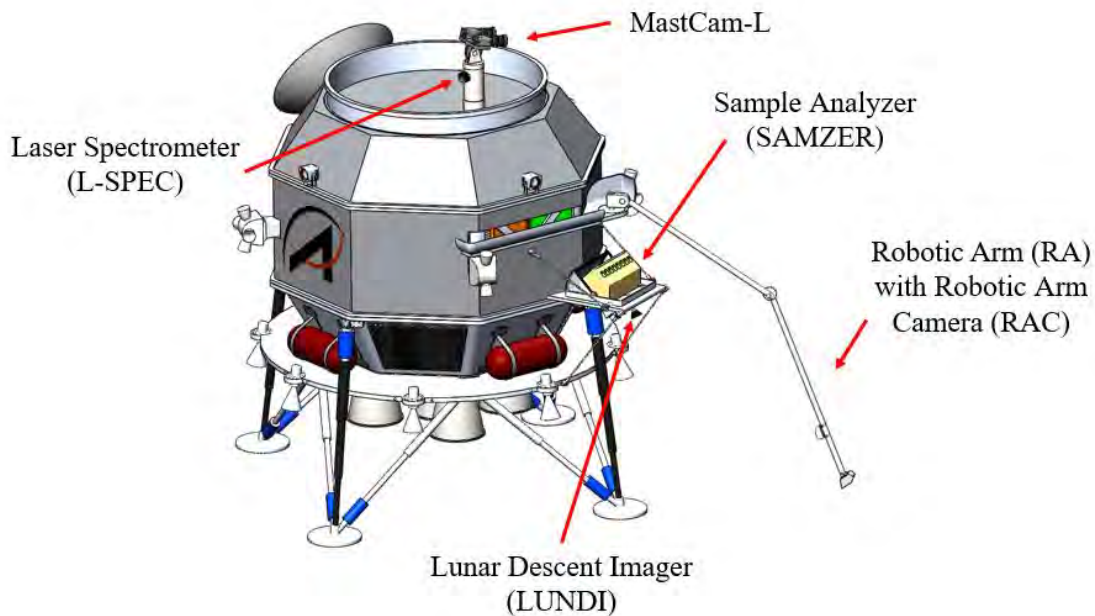
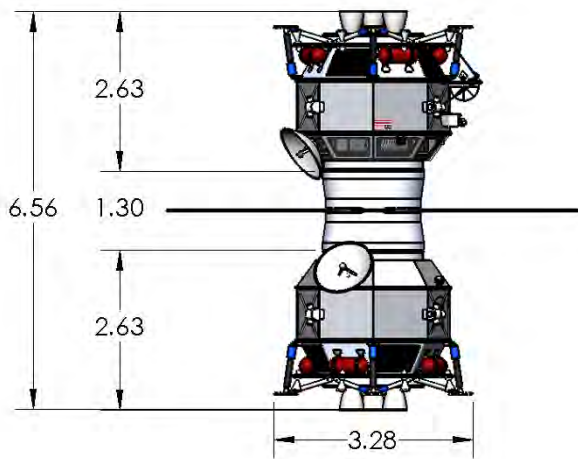
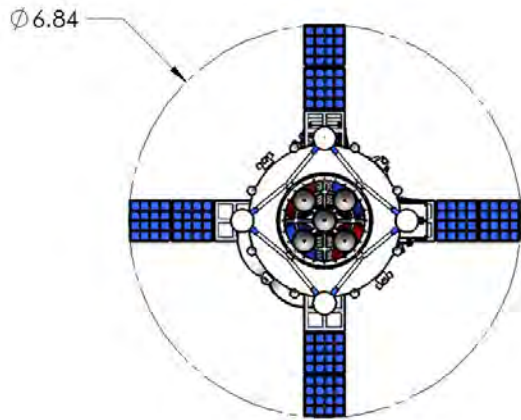


Figure 1-2: Lander Payload Instruments



*Stowed Configuration
(shown in SpaceX Falcon 9 standard fairing)*



Flight Configuration with Maximum Dimensions (m)

Spacecraft Maximum Height	6.56 m
Spacecraft Wet Mass	4439 kg
Coupler Total Height	1.30 m
Coupler Mass	260 kg
Individual Lander Maximum Height	2.63 m
Individual Lander Nominal Wet Mass	2021 kg
Individual Lander Nominal Dry Mass	759 kg
Launch Vehicle	SpaceX Falcon 9 Full Thrust
Launch Date	01-Apr-2022
Lunar Orbit Arrival Date	06-Apr-2022
Lunar Landing Date	06-Apr-2022
Science Mission Duration	10 days for each lander
Total Mission Cost (FY17)	\$493 M

Figure 1-3: Spacecraft Summary Sheet

2 Science and Instrumentation

2.1 Science Overview and Historical Context

Ever since the Apollo era, lunar water has been of great interest due to its implications for future space exploration. Water is one of the hardest to transport, yet most vital, resource for human space exploration. The discovery of a significant and concentrated amount of water in certain permanently shadowed regions of the Moon may enable future missions to harvest the water ice from the lunar regolith so that it can be used by astronauts, significantly lowering the mass and cost of missions and making lunar habitation (the creation of bases on the moon) cost-effective.

Lunar water was first discovered in samples brought back by the Apollo missions and its presence was confirmed by further American and Soviet missions. In 2009, Chandrayaan-1 and the Lunar Reconnaissance Orbiter provided conclusive proof that water ice was present over large areas on the Moon with the data obtained showing that many polar craters were likely to hold fairly large amounts of it, as shown in Figure 2-1 below. Due to its implications in space exploration, lunar water has become a point of focus for near-future space missions.

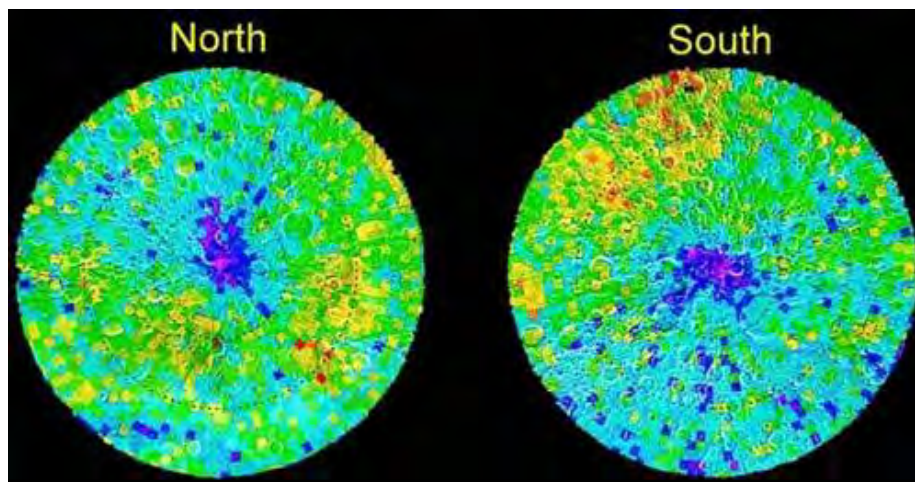


Figure 2-1: Hydrogen Concentration at Lunar Poles (Courtesy of Isaacson, Peter)



2.2 Landing Site Selection

Landing, sampling, and transmitting data from within permanently shadowed craters on the Moon poses a unique set of challenges. To accomplish this, the landing sites had to satisfy two essential criteria:

- 1) They must have strong indication of water ice already present, and
- 2) They must permit a method of transmitting data to the Earth's ground station

Communication could be achieved with an orbiter to relay data, but this proved too costly. The solution utilized by this architecture was to select landing sites that permit direct Lunar-surface-to-Earth communications based on allowable geometry while meeting the criteria for indicated presence of water ice.

To permit direct communications from the lunar surface, the Earth ground station elevation angle relative to the lander must eventually be greater than the crater rim-to-floor elevation angle. Data from the Lunar Impact Crater Database was analyzed and referenced with Systems Tool Kit (STK) geometry simulations to select the craters. From this analysis, the craters Scott and Nobile were chosen as they met all requirements set forth. The properties of these two craters are shown in Table 2-1

Table 2-1: Properties of the Selected Craters, Scott and Nobile

Crater name	Diameter [km]	Latitude [°]	Longitude [°]	Rim to floor depth [km]	Crater Elevation [°]	Max Antenna Elevation [°]	Strong Indication of Water Ice Presence?
Scott	107.82	-82.35	48.52	4.27	4.53	10.80	YES
Nobile	79.27	-85.28	53.27	3.89	5.61	8.83	YES

Crater selection also determines the science mission window, as these craters are not always visible from the ground station. The following figures, Figure 2-2 and Figure 2-3, show the ground station access for both craters, leading to the determination of the science mission time window.

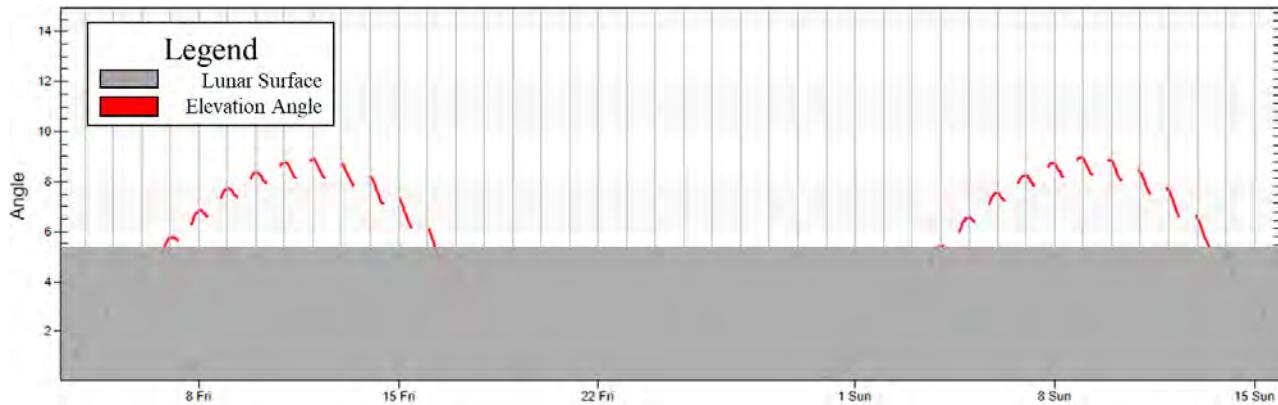


Figure 2-2: Communications Access for Crater “Nobile”, April-May 2022

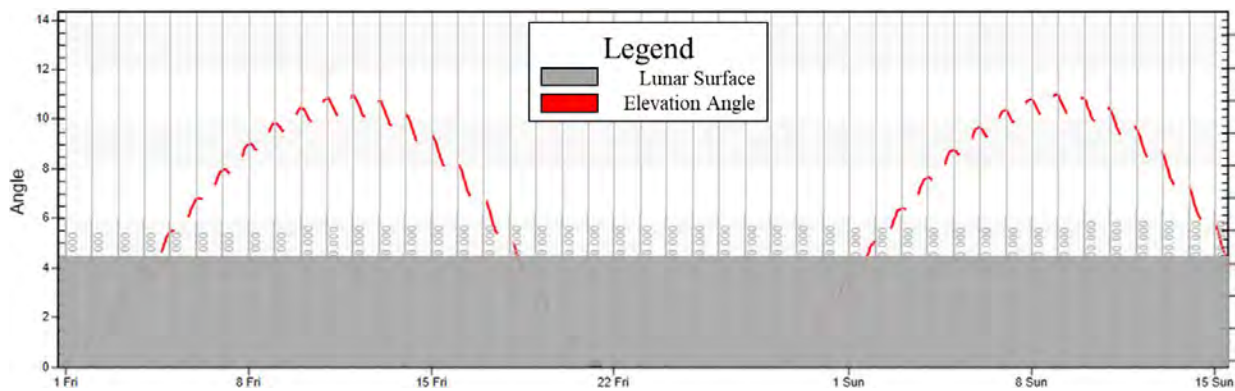


Figure 2-3: Communications Access for Crater “Scott”, April-May 2022

These access windows demonstrate that the optimum time for a science mission in April 2022 is from April 6th to April 16th. The ground station is visible for 12 hours each day during this timeframe. If this window is missed, the mission will have to be delayed until the May 1st when the window opens back up again.

Craters *Scott* and *Nobile* are both located near the Moon’s southern pole and are ~300 km away from the impact site of LCROSS. In October 2009, the impact of LCROSS with the lunar surface provided direct evidence of water ice in its ejecta plume.

There is also further indication of water ice presence in these craters. Figure 2-4 below, originally from “*Diviner Lunar Radiometer Observations of Cold Traps in the Moon’s South Polar Region*” by Paige et al., illustrates areas with the highest probability of trapped water ice. Using data gathered by LRO’s Diviner instrument, the authors created models that define locations where water ice can be trapped on the surface, and to what depth. The light blue regions indicate areas of permanent shadow, permitting the existence of near surface water ice. Within our chosen

craters Scott and Nobile, large areas of these regions exist, providing extremely strong indication of near surface water ice.

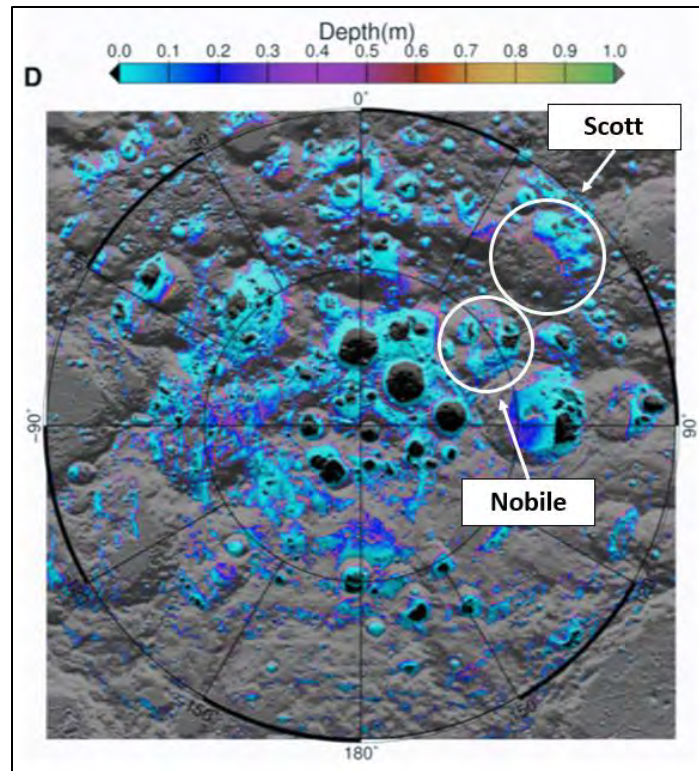


Figure 2-4: Areas of Strongest Indicated Water Ice Presence in the Lunar South Pole¹

2.3 Payload Instrumentation and Trade Studies

2.3.1 Robotic Arm (RA) and Robotic Arm Camera (RAC)

The Diana Robotic Arm, shown in Figure 2-5, is a 4-degree of freedom system designed to operate in the harsh environment of the permanently-shadowed lunar craters. It is essential to the mission as it is used to collect samples for analysis in SAMZER. It is equipped with a scoop with a front blade and back rasp to collect soil samples down to a depth of approximately 15 cm and transfer them to SAMZER for analysis. The rasp is powered by a motor so that it can cut through icy regolith. In addition to collecting samples for analysis in the SAMZER instrument, the RA is equipped with the Robotic Arm Camera (RAC), shown in Figure 2-5, to collect pictures of the trenches dug by the scoop using different filters (provided by a 3-color LED system); this gives the system the ability to provide visual data for the regolith and any larger water ice deposits as they are being dug up. The RA payload was chosen due to its ability to extend the sample-collecting area in comparison with a static system such as a drill (which was the alternative

payload option). A drill also presents other technical challenges, such as maintaining low temperatures during the drilling process to prevent sublimation of samples. For our purposes of sampling water ice, lunar drills do not yet possess a sufficient Technology Readiness Level (TRL). The performance characteristics of both the RAC and RA are shown in Table 2-2.

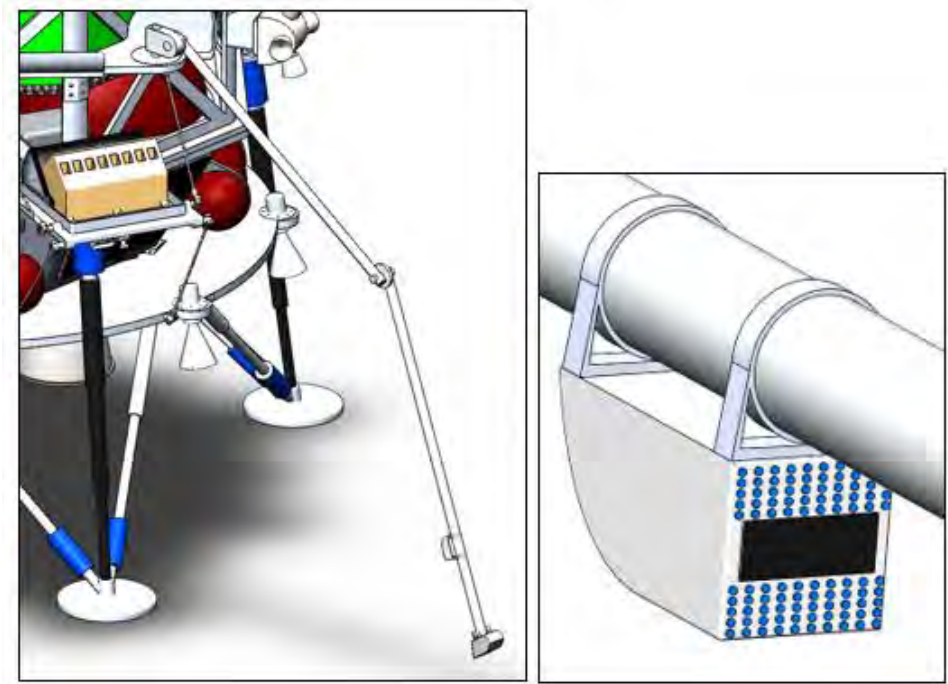


Figure 2-5: Robotic Arm (“RA”) Assembly (Left), Robotic Arm Camera (“RAC”, right)

Table 2-2: Specifications of RA and RAC Instruments

INSTRUMENT	MASS (kg)	PEAK POWER (W)	AVERAGE POWER (W)	AVERAGE DATA RATE (bps)
Robotic Arm (RA)	4.3	20.0	18.0	500
Robotic Arm Camera (RAC)	0.6	13.5	8.0	20,000

2.3.2 Sample Analyzer (SAMZER)

Primary sample analysis will be performed with Sample Analyzer (SAMZER) instrument, shown in Figure 2-6, is based heavily on the Thermal and Evolved Gas Analyzer (TEGA) from the Phoenix Mars Lander mission. Equipped with 16 individual ovens, SAMZER will have the capability of baking 16 discrete samples received from the Robotic Arm and then transferring the evolved gasses from those samples to its mass spectrometer and gas chromatographer.



This instrument will provide accurate quantification of water present in its samples, as well as key volatiles such as hydrogen and hydroxide. The performance characteristics of SAMZER are shown in Table 2-3.

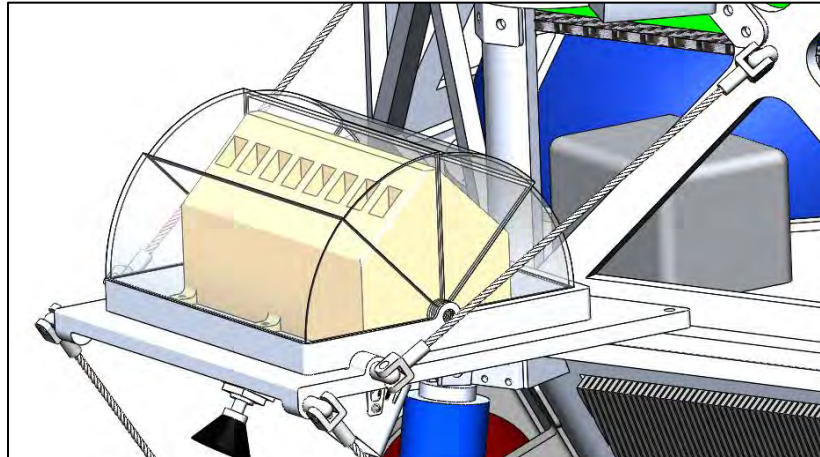


Figure 2-6: SAMZER Instrument Shown in its Retractable Protective Housing

Table 2-3: Sample Analyzer (SAMZER) Specifications

INSTRUMENT	MASS (kg)	PEAK POWER (W)	AVERAGE POWER (W)	AVERAGE DATA RATE (bps)
Sample Analyzer (SAMZER)	12.0	120.0	85.0	80,000

2.3.3 MastCam-L with Spotlight

The payload instrument MastCam-L, as seen in Figure 2-7, is based on MastCam-Z which will be on the Mars 2020 rover. Previous MastCam system was used on the curiosity rover and the details can be found below in Table 2-4. One different thing against the MastCam-Z is that the MastCam-L requires a spotlight attached with it due to darkness within the crater itself. The capability of the MastCam-L will include zoom, focus, as well as take 3-D pictures and videos. This allows detailed examinations of distant objects within the crater which can be used for further scientific research. The high resolution, stereoscopic images will also provide the general public breathtaking views of our nearest celestial neighbor, and perhaps even encourage some children and young adults to pursue engineering and the sciences.

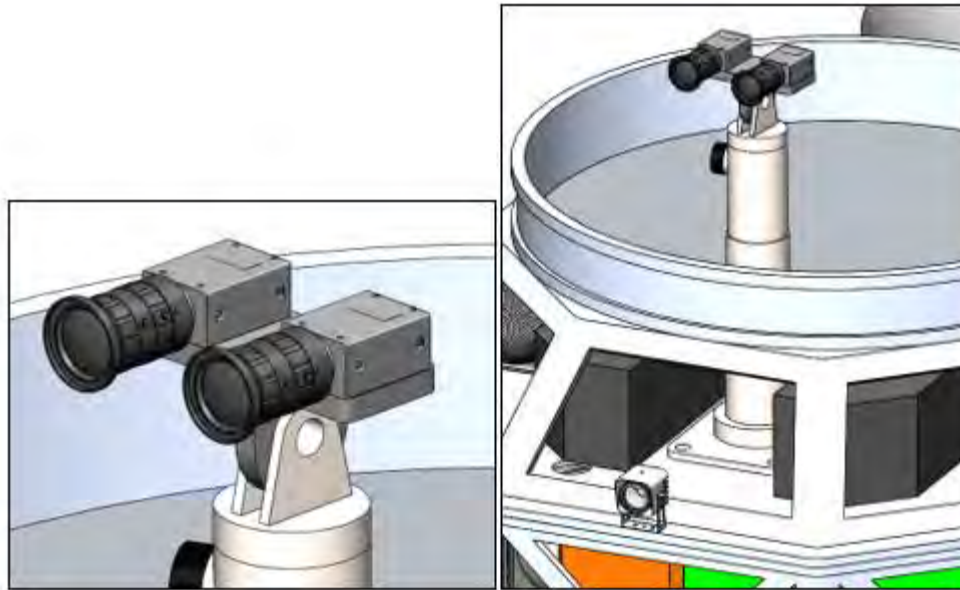


Figure 2-7: MastCam-L With Spotlight

Table 2-4: MastCam-L With Spotlight Detailed Information

INSTRUMENT	MASS (kg)	PEAK POWER (W)	AVERAGE POWER (W)	AVERAGE DATA RATE (bps)
MastCam-L with Spotlight	4.0	45.0	17.4	40,000

2.3.4 Lunar Descent Imager (LUNDI) with Spotlight

The Lunar Descent Imager (LUNDI) shown in Figure 2-8 is based on the MARDI design from the Phoenix Lander and Mars Science Laboratory (MSL) missions to Mars. Detailed information for the instrument is shown in Table 2-5. Because the camera was used on previous missions, it is a proven platform for providing vision as the lander descends toward the crater. LUNDI also requires a spotlight because once the lander enters the crater, it will be too dark to see the descent. This camera will allow visibility on the ground as the lander descends to see the conditions of the ground before landing. The LUNDI will provide interesting images which may provide additional scientific information on DIANA-I and II's descent.

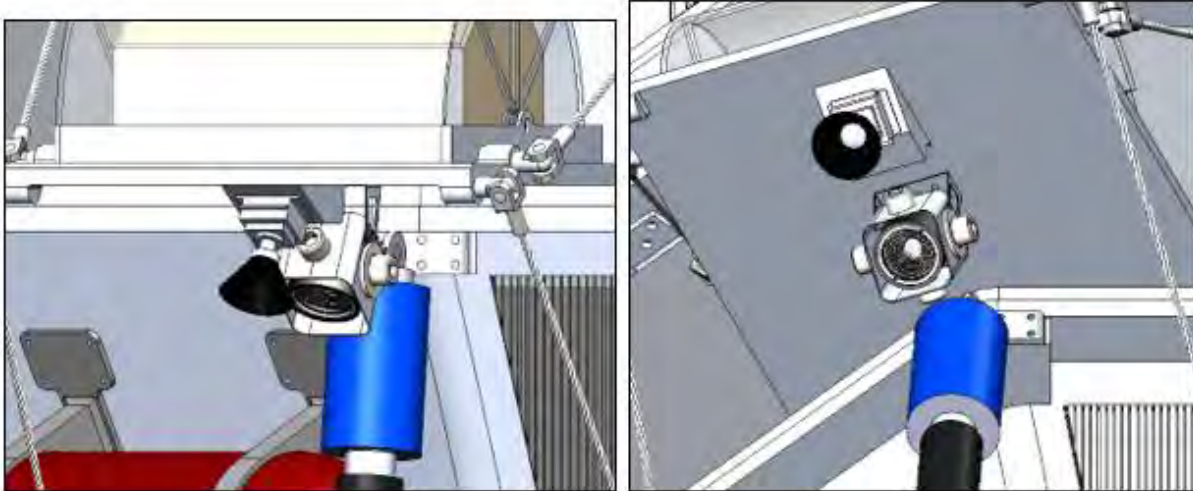


Figure 2-8: LUNDI Position Under SAMZER

Table 2-5: LUNDI Detailed Information

INSTRUMENT	MASS (kg)	PEAK POWER (W)	AVERAGE POWER (W)	AVERAGE DATA RATE (bps)
Lunar Descent Imager (LUNDI) with Spotlight	0.5	23.5	17.4	20,000

2.3.5 Laser Spectrometer (L-SPEC)

The L-SPEC instrument, shown in Figure 2-9, is a multi-band laser spectrometer capable of taking measurements near the 3.0 μm wavelength and has the characteristics shown in Table 2-6. For surface water in abundances of 0.01%, and the 1.6 μm wavelength, sensitive to ice abundances of about 1% ; the reflectance of water at these wavelengths can be seen in Figure 2-10². Thus, the readings will be able to show the location and quantity of water in the analyzed craters. The instrument can not only analyze the area surrounding the spacecraft after landing, but it can also scout for promising landing sites offering a resolution of 100 m when used from orbit. Compared to ChemCam, this system offers much greater range (ChemCam’s range is 7 m) and can detect water at multiple abundances. Due to its characteristics, L-SPEC will greatly aid the mission by providing optimal landing areas for sample collection and it will also make it possible to create a map of the concentration and location of lunar water in the craters analyzed.

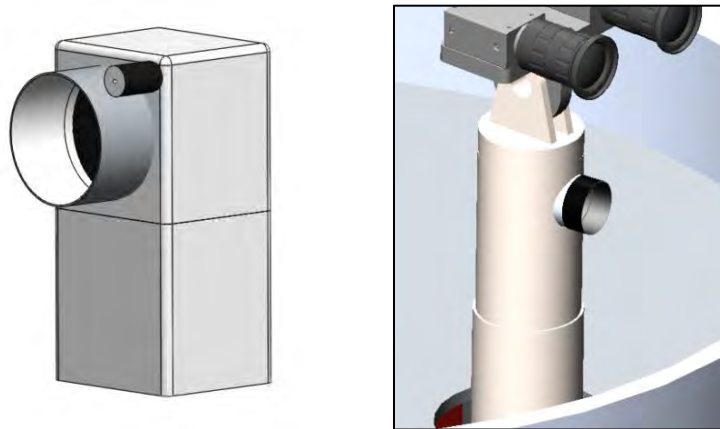


Figure 2-9: L-SPEC and Position Under MastCam-L

Table 2-6: Specifications for the L-SPEC Instrument

INSTRUMENT	MASS (kg)	PEAK POWER (W)	AVERAGE POWER (W)	AVERAGE DATA RATE (bps)
Laser Spectrometer (L-SPEC)	7.4	25.0	17.0	1,500

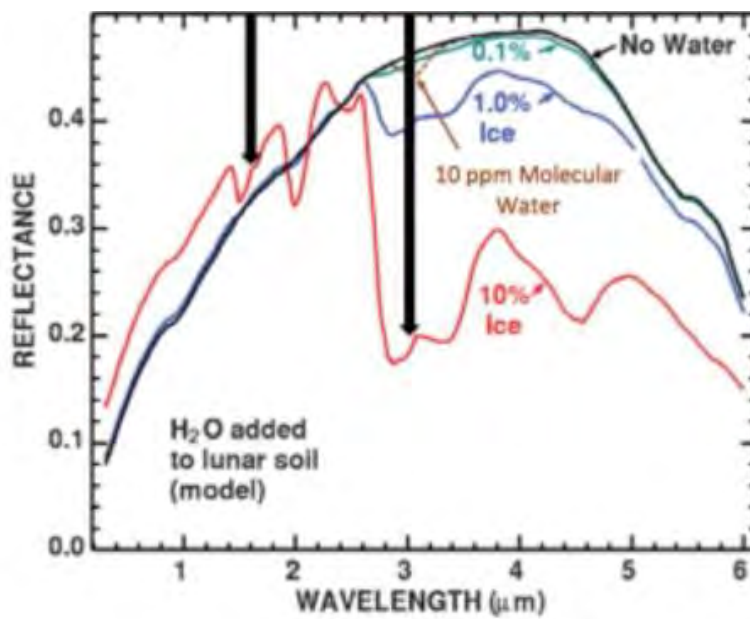


Figure 2-10: Reflectance of Water Relative to Wavelength, with Used Wavelength Marked²



2.4 Traceability to Requirements

To show that the selected instrumentation each have a purpose onboard the spacecraft, each instrument was linked to a requirement set forth in the RFP. The linked instruments to RFP requirements, with justification, is shown in Table 2-7.

Table 2-7: Traceability of Payload Instrument Selection to RFP Requirement

Rq. #	Requirement Text	Instruments	Explanation
00.0.001	Mission shall determine the locations and quantities of water deposits in terms of the ratio of water to regolith in two lunar craters.	Robotic Arm	Robotic Arm will sift through the lunar surface to bring up samples.
		Robotic Arm Camera	Get a close-up view of the samples so visual analysis can be done.
		SAMZER (Sample Analyzer)	The SAMZER analyzes the sample brought up by the robotic arm
00.0.006	Mission and design trade studies shall be weighted to prioritize using tech. that have already demonstrated on previous missions or are otherwise in the NASA technology development portfolio and are to be assessed on the basis of benefit, risk and cost	All payload instruments onboard the spacecraft	All instruments used on the spacecraft has been flown in previous mission. Some are being upgraded for use in future missions.
00.1.003	Mission shall maximize scientific data return before the end of the mission date of December 31, 2024.	LUNDI	LUNDI will provide images during descent to provide more closeup information about the crater.
		MASTCAM-L	This camera is for additional images as well as scoping out additional sites within the crater.
		SAMZER	SAMZER is the primary instrument for analyzing samples dug up by the robotic arm.
		RAC (Robotic Arm Camera)	RAC will provide closeup images of the samples being provided to the SAMZER for additional analysis.



2.5 Instruments Summary

A summary of all payload instruments is shown in Table 2-8.

Table 2-8: Payload Instrument Mass, Power, and Data Rates Summary

LANDER PAYLOAD INSTRUMENT	DESCRIPTION	REFERENCE INSTRUMENT (SOURCE MISSION)	MASS (kg)	PEAK POWER (W)	AVERAGE POWER (W)	AVERAGE DATA RATE (bps)
MastCam-L w/ Spotlight	Mast-mounted camera system with zoom functionality	MastCam-Z (Mars 2020)	4.0	45.0	17.4	40,000
Lunar Descent Imager (LUNDI) w/ Spotlight	Imaging assembly for descent	MARDI (Mars Polar Lander)	0.5	23.5	3.5	20,000
Laser Spectrometer (L-SPEC)	Laser spectrometer to survey nearby area for water	ChemCam (Curiosity)	7.4	25.0	17.0	1,500
Sample Analyzer (SAMZER)	Sample heating and mass spectrometer analysis	TEGA (Phoenix)	12.0	120.0	85.0	80,000
Robotic Arm (RA)	Scrapes surface to collect regolith samples	Robotic Arm (Phoenix)	4.3	20.0	18.0	500
Robotic Arm Camera (RAC)	Lighted camera to provide close-up visuals of samples and trenches	RAC (Phoenix)	0.6	13.5	8.0	20,000
LANDER PAYLOAD TOTALS			28.8 kg	247.0 W (PEAK)	163.9 W (AVG)	161,500 bps (AVG)





3 Mission Design

3.1 Launch Vehicle Trade Study and Selection

Getting to space is an expensive endeavor, and launch costs are typically the largest line item expense for any mission. A launch vehicle trade study was performed that sought to reduce cost while maintaining high likelihood of success for a translunar injection trajectory. For our design, a “heavy lift” vehicle was not necessary, and this alone results in significant cost savings. To achieve our desired C3 of $-1.95 \text{ km}^2/\text{s}^2$, our choices came down to the ULA Atlas V 400 series and the SpaceX Falcon 9 Full Thrust. Table 3-1 summarizes the relative advantages and disadvantages for each platform.

Table 3-1: Launch Vehicle Comparison

ULA Atlas V 400 Series	SpaceX Falcon 9 Full Thrust
 <ul style="list-style-type: none"> • Extremely capable system with efficient LOX/LH2 Centaur Upper Stage • Proven track record with 76 successful launches out of 77 • Features such as payload separation systems come standard • Customer friendly, detailed Payload Planner’s guides • Expensive: \$140M FY 2022 expected launch cost 	 <ul style="list-style-type: none"> • Similar capabilities to ULA Atlas 400 series • 51 successful launches out of 53 • No standard-service payload separation systems • Limited amount of performance information available to public • Much lower expected cost: \$72M FY 2022

SpaceX provides the most cost-efficient option by far, and we have selected the Falcon 9 Full Thrust as our launch vehicle. There are some inconveniences associated with the choice however. Since publicly available performance information is limited, and SpaceX was unresponsive to our inquiries, we were forced to interpolate a lift capability of 5400 kg to our C3. This value was cross-referenced with the similar performance of the Atlas V 400



series, but without more detailed information from SpaceX, it's hard to know how accurate this derived value is. However, although the lack of detailed payload planning information is inconvenient, the millions of dollars saved by going with SpaceX makes it worth it.

3.2 Mission Operations Timeline

The following table, Table 3-2, outlines the CONOPS for the lunar mission timeframe.

Table 3-2: CONOPS Stage Detail

CONOPS Stage	ΔV	Time in Stage	Propulsive Craft	Date/Time of Event (UTCG)
1: Launch to LEO	9.3 km/s	45 minutes	Falcon 9 FT	1 Apr 2022 20:01:10.390
2: Translunar Injection	3.11 km/s	4 days 10.5 hours	Falcon 9 FT	1 Apr 2022 20:45:54.083
3-B1: Lunar Capture 1	390 m/s	110 seconds	DIANA-I	6 Apr 2022 07:21:57.306
3-Coast to Capture 2	-	7 hours	-	-
3-B2: Lunar Capture 2	430 m/s	105 seconds	DIANA-II	6 Apr 2022 14:21:47.298
4: 50 km Lunar Parking Orbit	-	4 hours 15 minutes	-	-
5-L1: Landing 1	1.85 km/s	530 seconds	DIANA-I	6 Apr 2022 18:38:21.511
5-IC: Coast to Landing 2/ Inclination Change	71 m/s	2 hours	DIANA-II	6 Apr 2022 20:09:08.597
5-L2: Landing 2	1.85 km/s	530 seconds	DIANA-II	6 Apr 2022 20:31:54.853
6: Science Mission	N/A	9 days 17 hours	N/A	16 Apr 2022 03:24:42.000

3.3 Trajectory Design

Two different lunar trajectories were considered for this mission. Most of the missions flown historically have used a direct ballistic transfer, approximately placing their spacecraft on a Hohmann transfer to the Moon. Few missions have flown different variations of low-energy transfer trajectories, either by using an ion drive or some other mechanism to reduce the spacecraft ΔV requirement. In 2012, NASA flew the Gravity Recovery and Interior



Laboratory (GRAIL) mission using a Lagrange point flyby to intercept the Moon at a more favorable speed for capturing into lunar orbit.

Comparing this mission and launch vehicle to GRAIL, unfortunately, doing a low energy transfer was not possible given this architecture. The low energy transfer requires much less mass from lunar capture insertion, but with the Falcon 9, the payload capability into this orbit is drastically reduced to approximately 2300 kg. Because of this, the ballistic trajectory was selected, despite more spacecraft fuel necessary to be carried.

3.3.1 CONOPS Stage 1: Launch to LEO

1 Apr 2022 20:01:10.390 UTCG

The mission launches from Cape Canaveral on a Falcon 9 into a parking orbit around the Earth with a 300 km parking orbit around the Earth. The second stage engine will have to ignite and shut down to complete this maneuver. From here, the spacecraft will coast until it is aligned with the proper spot to start the translunar injection maneuver.

3.3.2 CONOPS Stage 2: Translunar Injection

1 Apr 2022 20:45:54.083 UTCG

After coasting in the LEO parking orbit, the Falcon 9 second stage MVac engine will reignite and consume the rest of the launch vehicle's fuel, placing the spacecraft on a trajectory to intersect with the moon. Before leaving the Earth's sphere of influence, we can perform a systems check with the currently existing Tracking and Data Relay Satellite System (TDRSS) to ensure that no damage has occurred during the launch phase.



3.3.3 CONOPS Stage 3: Lunar Capture

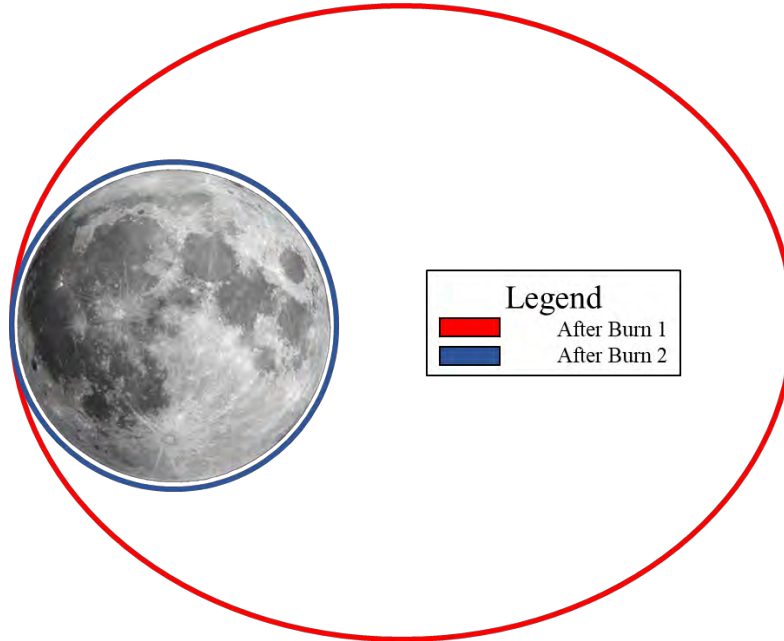


Figure 3-1: To-Scale Resultant Orbits from Lunar Capture Burns

6 Apr 2022 07:21:57.306 UTCG

After 5 days of coast time, the landers will reach perilune, 50 km from the surface of the moon. DIANA-I will perform a burn with a ΔV of 390 m/s to capture it into an elliptical orbit around the moon. This orbit has an inclination of 97.7° and an eccentricity of 0.58, safely placing it out of the influence of the Earth's gravity and fully capturing around the Moon. This orbit has a period of 7 hours. During these 7 hours, the spacecraft will rotate 180° to execute a second burn.

6 Apr 2022 14:21:47.298 UTCG

DIANA-II performs the second capture burn, with a ΔV of 430 m/s. This maneuver consumes the almost the same amount of fuel as the above burn, leaving the landers symmetrical in tank size. The landers have reached their circular lunar parking orbit with 50 km altitude. From here, the landers will coast directly over the first crater, Scott.



3.3.4 CONOPS Stage 4: Lunar Descent

6 Apr 2022 18:38:21.511 UTCG

DIANA-I will detach from the coupled system and begin its descent into the crater Scott. The thrusters will fire at a constant value for thrust for 530 seconds directly opposite to the current velocity vector. It is aided by attitude control with LiDAR to calculate its own velocity with respect to the moon. This maneuver has an equivalent ΔV of 1.86 km/s.

6 Apr 2022 20:09:08.597 UTCG

DIANA-II performs an inclination change to align it with the second crater, Nobile. This maneuver has a ΔV of 71.3 m/s.

6 Apr 2022 20:31:54.853 UTCG

DIANA-II performs the exact same landing maneuver as detailed above.

16 Apr 2022 03:24:42.000 UTCG

The bottom of crater Nobile is no longer visible from WSGS and will not be visible for the rest of the moon's rotation. DIANA will not be visible again until May 4th. This marks the end of the science mission.

3.3.5 Backup Trajectories

The moon cycles around the Earth every 28 days. This trajectory can be repeated in a month should an emergency arise. Any minor delays would take up time on the science mission. Our Earth parking orbit has a period of 1.5 hours, allowing for any emergency maintenance should we miss our initial Translunar Injection (TLI) burn. The period of our Lunar orbit is 1.9 hours, which permits additional maintenance time if the systems are not ready to land in our timeframe window.

3.4 Landing and Hopping Detail

The purpose of the lunar hop is to expand the capabilities and reach of each lander. By being able to move to another landing site, the lander can evaluate the regolith composition in an area far beyond just the reach of the robotic



arm. This design provides the mobility of a rover along with the size and reliability of a lander. Since there are only two landers travelling to two separate craters, being able to assess as much of the crater as possible is a driving factor.

In order for the lunar hops to be feasible, the landers must be equipped with capable thrusters to land and launch the vehicle along with sufficient propellant for three hops and the final stage of the initial descent from orbit. Since the scientific mission of this architecture is to analyze the regolith for water concentrations, the lander cannot risk contaminating the regolith before it has been sampled by the robotic arm. Monopropellant Vernier thrusters are included on the landers to mitigate the contamination risks associated with the main engine bipropellant thrusters. While the bipropellant engines' plume generates water in its exhaust, the monopropellant thrusters do not.

The landing and lunar hop phase begins with the lander shutting down the main engines at 150 meters above the lunar surface to reduce the risk of water contamination. Immediately afterwards, the Vernier engines ignite to further slow the landers' descent from 22 m/s to 1 m/s until touchdown. Upon completion of the scientific mission at this landing site, the main engines will burn for roughly one second, enough to boost the lander back up to about 150 meters. Once at this altitude, the Vernier engines reignite to slow down the lander once again. Throughout this process, the ACS thrusters are firing to shift the lander horizontally across 150 meters. This sequence is depicted in the following diagram, Figure 3-2.

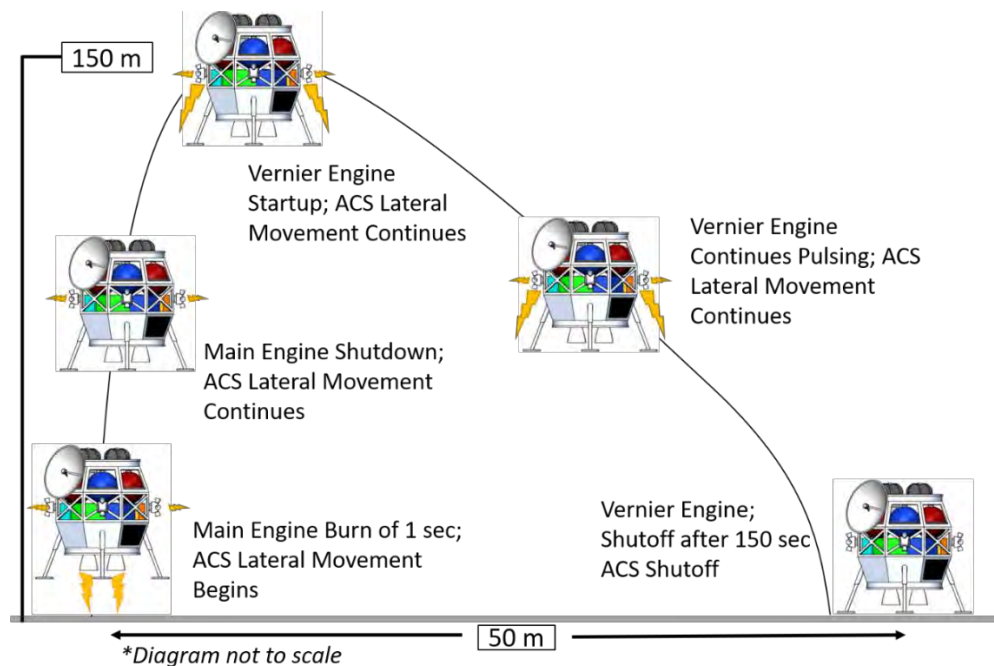


Figure 3-2: Lunar Hop Sequence

3.5 CONOPS Stage 5: Science Operations

3.5.1 Science Operations Flowchart

Once landing in their respective sites, each lander will follow a strict set of rules to begin the scientific analysis of the areas regolith. This process is shown as a flow chart in Figure 3-3.

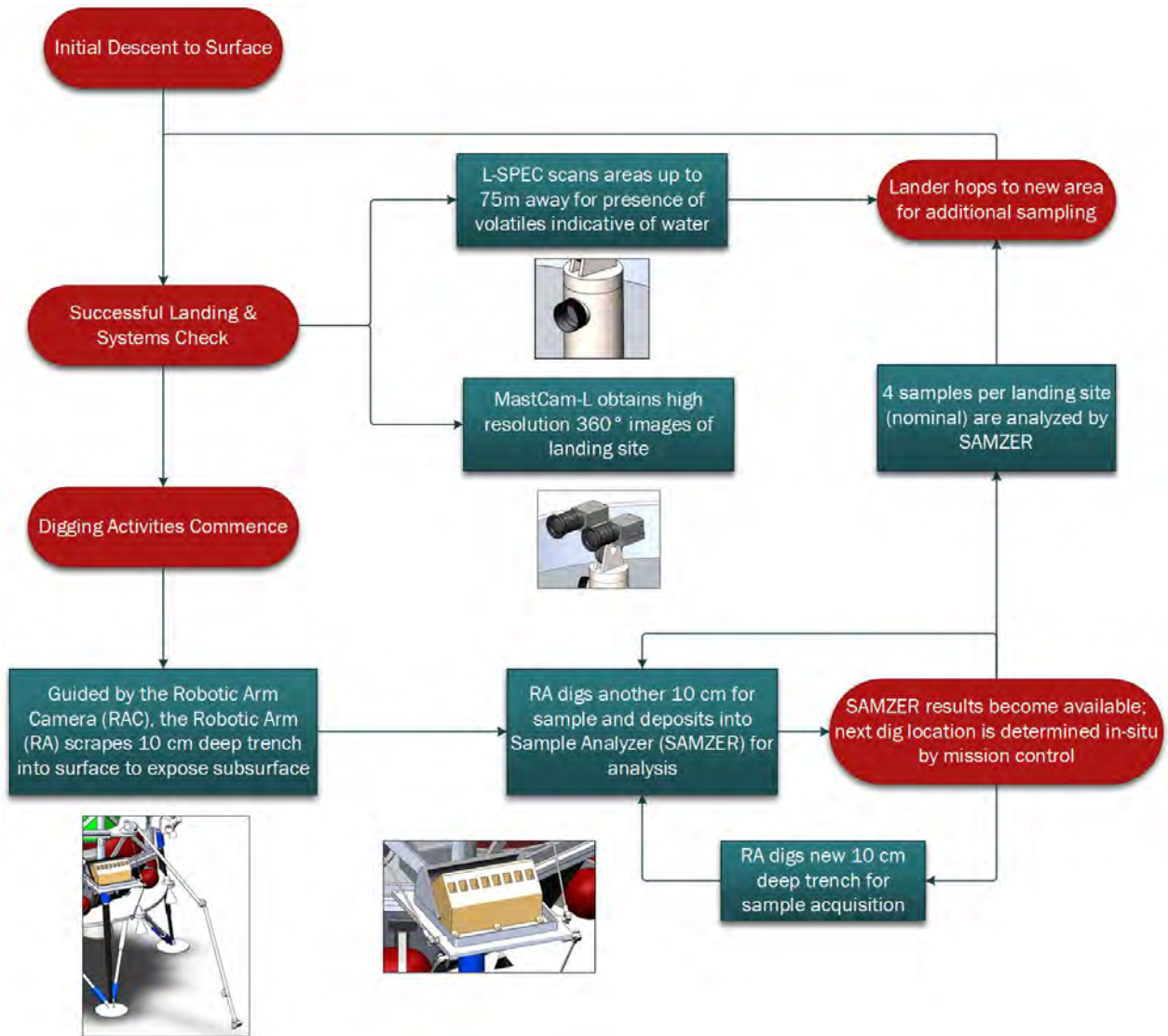


Figure 3-3: Illustrated Science Operations Flowchart

3.5.2 Data Return

DIANA has a window of opportunity for half of the day during our science mission to return the data. The mission data return rate is 20 Mbps, which allows for data transfer to either White Sands, New Mexico, or Wallops Island,



Virginia without having to throttle the data rate. At this data rate, DIANA will need to downlink for an hour each communication window to avoid filling the onboard solid-state drives.

3.6 End of Mission

The end of the spacecraft's mission is characterized by passivation and disposal through various methods. Although there are no requirements on how this is accomplished, there are strong recommendations published by the Inter-Agency Space Debris Coordination Committee on how spacecraft should be disposed of on the Moon. These recommendations include minimizing the possibility of collisions and explosions, avoiding orbits longer than 10 years, and the passivation of orbital hardware. Lastly, these goals shall be accomplished with planetary protection protocols taken into account as well.

3.6.1 Planetary Protection Protocols

Since this mission is targeted to go to Earth's moon, it falls under category II planetary protection protocols. This is defined as there being a very low likelihood of forward contamination on the lunar surface, and thus minimal steps need to be taken to ensure the spacecraft is compliant.

3.6.2 Spacecraft Disposal

Since this spacecraft is comprised of the two landers and a coupler, each will have its own method of disposal. After detachment from the landers, the coupler is left in a decaying orbit that will impact the moon after 76 days on the far side of the moon, away from any historical sites. Upon mission completion, each lander will begin venting its propellant and pressurant. Once the propellant and pressurant have been vented, the fuel cells can begin their venting as well. Due to the absence of an atmosphere on the lunar surface, all liquid will boil rather quickly. Gauges along the feed lines will provide real-time monitoring of the amount being vented. Since the solar arrays are attached to the coupler, there is no additional possibility of the lander's systems being charged after venting.



4 Spacecraft Sub-System Design

4.1 Configuration and Field of View (FoV) Plots

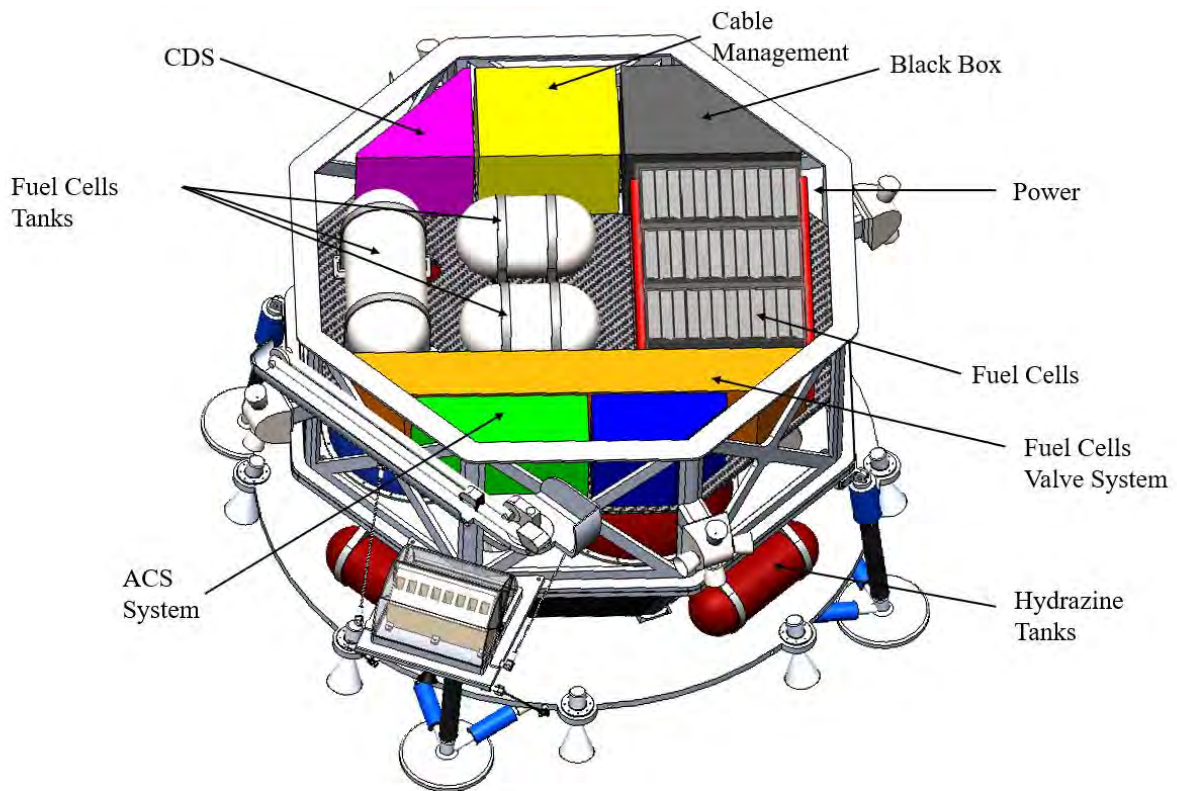


Figure 4-1: Spacecraft Internal Configuration

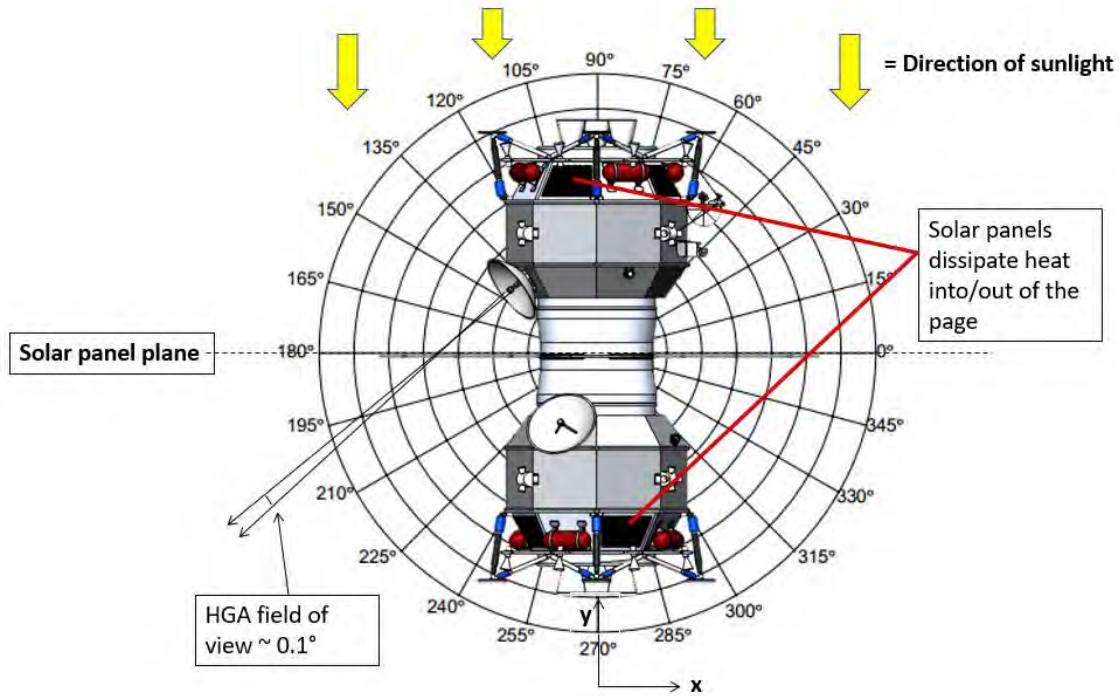


Figure 4-2: Bus Component FoV Plot

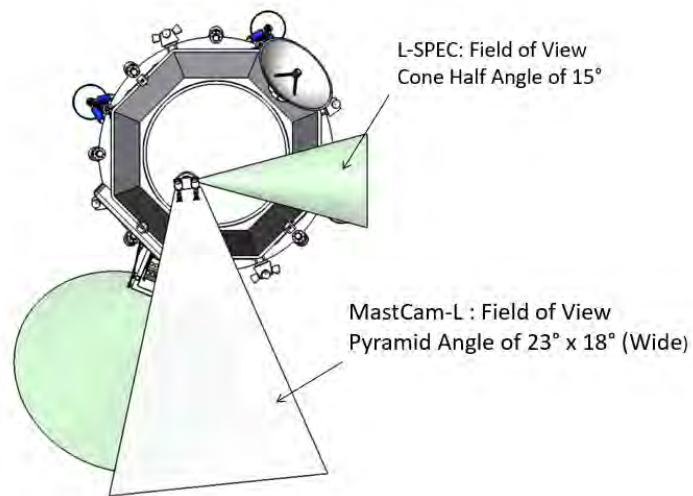


Figure 4-3: FOV Plots for L-SPEC and MastCam-L Payloads

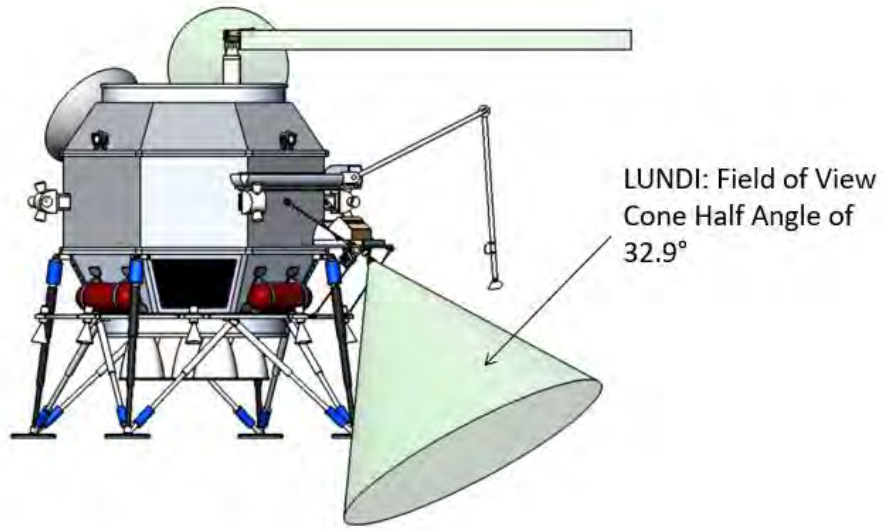


Figure 4-4: Field of View for Lunar Descent Imager

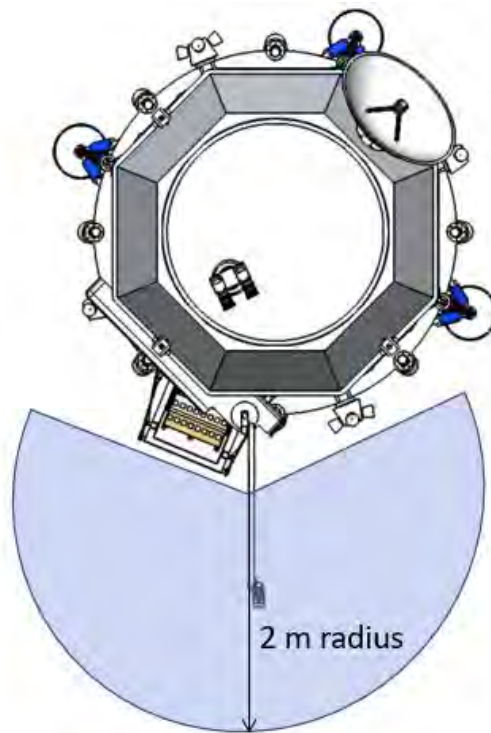


Figure 4-5: Robotic Arm Range

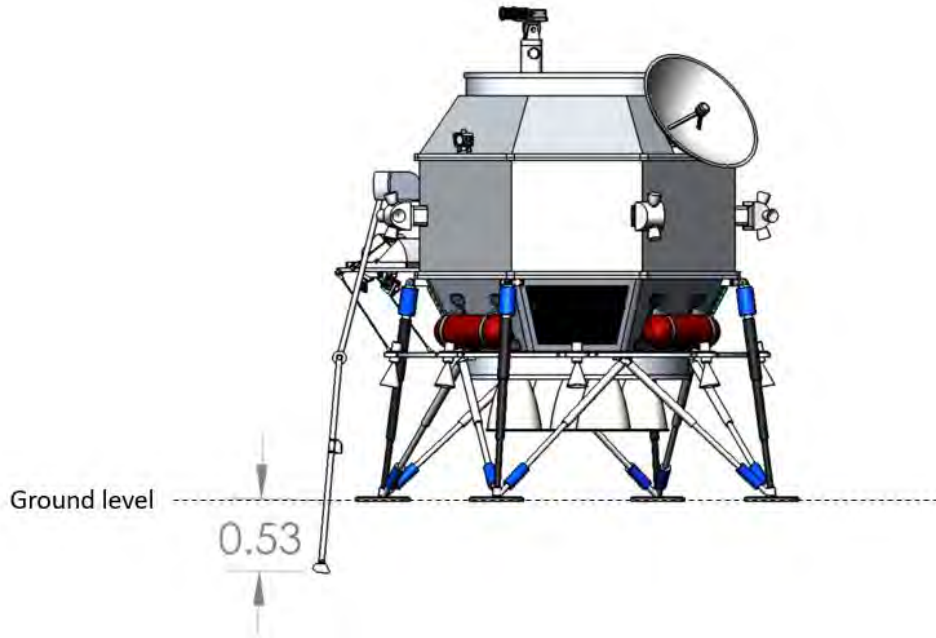


Figure 4-6: Robotic Arm Maximum Depth Achievable (meters)

4.2 Propulsion

4.2.1 Propulsion Requirements

The design of the propulsion subsystem begins with defining the requirements needed to be fulfilled by the subsystem, listed below on Table 4-1.

Table 4-1: Propulsion System Driving Requirements

Req. No.	Requirement Text
4.2.1	Propulsion system shall deliver at least 2.5 km/s of ΔV per lander
4.2.2	Propulsion system shall be capable of restarting and operating within their lifetime capacity
4.2.3	Propulsion system shall reduce and, if possible, eliminate the risk of water contamination

4.2.2 Propulsion Subsystem Trade Study

To meet these requirements, several propulsion options were explored, which included bipropellant and monopropellant engines, solid motors, and electrostatic engines.



Electrostatic engines offer a high efficiency with Isp values upwards of 1310 seconds, but their low thrust capabilities and high-power consumption limit the phases of the mission during which it can be used. Additionally, to be able to compensate for the high-power consumption, an RTG would need to be incorporated to the design. Aside from the lander redesign problems this creates, an RTG is roughly \$110 million (FY2018), more than a fifth of the mission's allocated budget. If an electrostatic engine were to be used, a liquid engine and ACS thrusters would still need to be incorporated for the landing phase and the lunar hops due to the high thrust requirements and low burn times.

Solid motors are another commonly used propellant due to their simpler design and moderate Isp values of about 220-250 seconds. These kick motors can be staged on the landers so that after each burn is completed, the spent kick motor can be jettisoned, reducing excessive mass. As was the case with the electrostatic engine, if a solid motor was to be used for the lunar capture and descent phases, a liquid engine and ACS thrusters would still be needed since solid motors cannot be throttled nor can they be restarted.

The last common spacecraft propulsion systems we considered were liquid engines, both as monopropellant and bipropellant engines. Monopropellant engines are simpler since it only needs half of the hardware that is typically found in a bipropellant system. The tradeoff comes with the lower Isp of about 220 seconds, resulting in additional propellant mass needed to complete the equivalent ΔV burns with a bipropellant engine. Bipropellants offer greater efficiency, about 300 sec, and can reach higher thrust regimes. Both types can be restarted, but bipropellant engines cannot suffice for minute ACS thruster control in the same form that monopropellant engines can. For this reason, the selected architecture has been designed as a dual-mode system, incorporating the benefits of both types of liquid engines.

Propellant selection for liquid engines is divided into two categories, storable and cryogenic. Cryogenic propellants tend to offer higher specific impulse and thrust values, but their temperature restrictions typically limit their usage to launch vehicles. While the mission duration of this architecture is approximately just 16 days, maintaining propellants at cryogenic temperatures throughout this duration adds extensive insulation and hardware requirements. Therefore, any cryogenic fuels were ruled out due to their added complexity. Storable propellants require less maintaining, leading to lower mass requirements. The most common propellants of this category are Nitrogen Tetroxide (NTO) and Hydrazine (HYD), which also have the benefit of being hypergolic and therefore do



not need an ignition system. Although hydrazine is very toxic and requires special handling, it is a propellant that has been used for many years already and any special procedures and equipment are readily available. Non-toxic propellants, such as hydroxylammonium nitrate (HAN), were considered, but to their early development stages cannot be justified to be used for this spacecraft architecture.

4.2.3 Main Engines

The main engine requirements are to maximize the thrust capability so that burn times are minimized and can be treated as instantaneous burns. The engines shall be capable of being throttled, restarting and have a sufficient lifespan to complete the designed mission. Each engine must deliver a total impulse of 3,805,000 N-sec and be capable of restarting. A trade study was done to review the engines being considered for the architecture, shown below in Table 4-2.

Table 4-2: Main Engine Trade Study³

Engine	Manufacturer	I_{sp} (sec)	Thrust (N)	Propellants
R-40B	Aerojet	320	4,000	HYD/NTO
R-42DM	Aerojet	327	890	HYD/NTO
LEROS 1b	Moog	317	635	HYD/MON
S400-15	Ariane Group	321	425	MMH/NTO

While each of these engines offered high I_{sp} values for liquid engines, only the Aerojet R-40B can produce the thrust necessary to minimize the burn time for the spacecraft. Each lander will utilize 5 R-40B engines operating at 80% thrust, allowing for mission completion with one engine out.

4.2.4 Vernier Engines

The Vernier engine requirements are to bring the landers to a soft landing of no more than 5 m/s while ensuring that the regolith is not contaminated by the engine's exhaust. For this reason, any bipropellant engine of Hydrazine and Nitrogen Tetroxide was ruled out. Instead, this landing system requires the use of monopropellants that do not produce water as a product. Each engine must deliver a total impulse of 175,000 N-sec and be capable of pulsing and restarting. As was done for the main engines, a trade study was conducted for final selection, shown below in Table 4-3.



Table 4-3: Vernier Thruster Trade Study

Engine	Manufacturer	I_{sp} (sec)	Thrust (N)	Propellants
MR-104 A/C	Aerojet	223	440	HYD
MR-107V	Aerojet	223	220	HYD
400N Class	Ariane Group	212	400	HYD
MONARC-445	Moog	234	445	HYD

The MONARC-445³ manufactured by Moog Aerospace was selected due to its high thrust and specific impulse. All of the engines evaluated were capable of delivering the required total impulse and along with capacity to restart and pulse. With the MONARC-445, 8 engines will be arranged along the base of the lander, with 4 only being needed to complete the mission.

4.2.5 Drop Tank Trade Study

In an effort to reduce the spacecraft mass and improve the design efficiency, two scenarios were considered for the lunar capture burn.

In the first scenario, the spacecraft would complete its pair of lunar capture burn with the assistance of “drop tanks” positioned within the coupler between the two landers. These propellant and pressurant tanks would only feed into the propulsion system of one of the landers in order to compensate for the propellant and pressurant lost during a full capture burn of 830 m/s. After the burn was complete and the landers separated, the coupler, along with the tanks, were to be jettisoned away before the final lander was to complete its descent to the lunar surface. Doing so would dispose of any unnecessary mass and require less propellant for the lander to slow down as well.

In the second scenario, the landers are still attached via a coupler, but there is no propellant or pressurant stored within it. Instead, the propellant needed for the capture burns is stored within each lander’s respective tanks and the lunar capture burn is divided up in to two segments. The first burn of 430 m/s is completed by Diana I, with Diana II completing the second burn of 390 m/s. With this scenario, the bare coupler was jettisoned, and the propellant tanks are maintained within the landers with added empty space, as opposed to the ones from the first scenario.

Although the first scenario produced a mass savings of about 370 kg, we found the second scenario with the internal tanks to be safer and more reliable. The additional plumbing required to route the pressurant and propellant from the coupler to the lander’s tanks created an unnecessary point of failure should the plumbing fail to separate from the lander and coupler. Additionally, while the first scenario may have been more efficient and cut down on mass, the



current architecture is well within the margin of the selected launch vehicle and can therefore suffice the added mass. It is noteworthy that in the event that spacecraft mass needs to be reduced, scenario one can be considered as a possible solution.

4.2.6 Tank Sizing

The sizing of the tanks begins with the calculation of the propellant masses. Beginning with a single lander's dry mass and the ΔV required for the final lunar hop, the Tsiolkovsky rocket equation is used to determine the amount of propellant needed. A 5% margin along with margins for residual propellant (2%), outage (1%) and loading error (0.05%) are added to the propellant mass for a sum total¹⁰. Using an O/F ratio of 1.42, the mass for the oxidizer and fuel can each be calculated, followed by the volume. The total propellant volume is then used to calculate the volume of helium required to maintain the propellants pressurized to 3.3 MPa, while the helium pressure ranges from 34.5 MPa to 3.8 MPa. The final result of this process is a mass value for both propellants and the pressurant needed to maintain those at the specified pressure. The process is outlined in Table 4-4 for the lander lunar descent.



Table 4-4: Propellant and Pressurant Mass Calculation

Constants	
ΔV by SC	1856 m/s
m_{burnout}	752.5 kg
I_{sp}	320 sec
O/F Mix Ratio	1.42:1
Propellant Densities @ 26.7 °C	
ρ_{NTO}	1450 kg/m ³
ρ_{HYD}	1021 kg/m ³
Descent Phase Propellant Mass & Volume	
m_{burnout}	752.5 kg
$m_{\text{Propellant}}$	606.6 kg
m_{Margin} (8.05%)	51.6 kg
Descent Phase Total Mass	658.2 kg
m_{NTO}	386.2 kg
$m_{\text{HYDRAZINE}}$	272.0 kg
Vol_{NTO}	0.3 m ³
Vol_{HYD}	0.3 m ³
Descent Phase Prop. Vol	0.5 m ³
Constants for Propellant Tanks	
Ullage	0.3
P_{max}	3.3 MPa
Constants for Pressurant Tanks	
P_{initial}	34.5 MPa
P_{final}	3.8 MPa
Helium Mass & Volume	
$\text{Vol}_{\text{helium}}$	0.1 m ³
m_{helium}	3.2 kg
Propulsion Mass Statement for Single Lander, Descent Phase	
$m_{\text{Propellants}}$	658.2 kg
m_{helium}	3.3 kg
Propulsion Wet Total	661.5 kg

This is then repeated for each stage of the mission, each time including the previously calculated masses as shown in Table 4-5.



Table 4-5: Propellant and Pressurant Mass per Lander

Diana 1				Diana 2			
	ΔV Req'd. (m/s)	$m_{propellant}$ (kg)	$m_{pressurant}$ (kg)		ΔV Req'd. (m/s)	$m_{propellant}$ (kg)	$m_{pressurant}$ (kg)
Lunar Capture Burn 1	390	515	6.1	Lunar Capture Burn 2	430	492	6.1
Lunar Descent	1856	658	3.3	Inclination Change	71.3	35.2	0.2
Lunar Hops (3)	129.3	77.1	0.4	Lunar Descent	1856	658	3.3
				Lunar Hops (3)	129.3	77.1	0.4
Total	2375.3	1250.1	9.8	Total	2486.6	1262.3	10

Once all the propellant and pressurant masses have been calculated, their respective tanks can be sized. A 30% increase in volume is accounted for and added to the volume of each individual propellant volume. Although the volume of propellants results in roughly the same amount due to the chosen O/F ratio and their respective densities, the hydrazine tank will require more volume to account for the lunar hops. Given this, all of the tanks are sized for the amount of hydrazine required for greater ease of manufacturing.

The propellant tanks are designed and calculated to be made from titanium while the pressurant tanks will be composite overwrapped pressure vessels (COPV). Titanium is suitable for the pressurant tanks as well, but the added mass needed to maintain the required pressure can be eliminated with the COPV. Table 4-6 below outlines the properties for both materials that were used to size each tank.

Table 4-6: Propellant & Pressurant Tank Constants

Titanium Tank Constants		COPV Constants	
Ullage	30 %	$P_{initial}$	34.5 MPa
P_{max}	3.3 MPa	P_{final}	3.8 MPa
$\sigma_{yield-Ti}$	1.06 GPa	$\sigma_{yield-CF-Al}$	848 MPa
$\rho_{Titanium}$	4430 kg/m ³	ρ_{CF-Al}	1800 kg/m ³

For both tanks, the internal radius is calculated from the volume of space needed and the equation for the volume of a sphere. The thickness is determined from the spherical stress equation and used to determine the outer radius. This process is outlined in Table 4-7 for both propellant and pressurant tanks. Each propellant tanks was sized to weigh about 30 kg and with a spherical outer radius of 0.56 m. The COPV tanks were sized to weigh 25 kg and have a spherical outer radius of 0.31 m.

Table 4-7: Titanium & COPV Tank Sizing

Titanium Tank Sizing		COPV Sizing	
Vol _{HYD}	0.72 m ³	Vol _{helium}	0.11 m ³
r _{internal}	0.56 m	r _{internal}	0.30 m
t	0.00 m	t	0.01 m
r _{outer}	0.56 m	r _{outer}	0.31 m
m _{tank}	29.81 kg	m _{tank}	25.32 kg

4.2.7 Propulsion Schematic

In all, the propulsion subsystem consists of 5 main engines, 8 Vernier thrusters and 12 ACS thrusters. The propellants, HYD and NTO, are pressure fed through a regulated system using helium while going through a series of check valves, filters and pressure regulators. Each propellant tank features an aluminum rolling diaphragm, similar to the one shown in Figure 4-7.

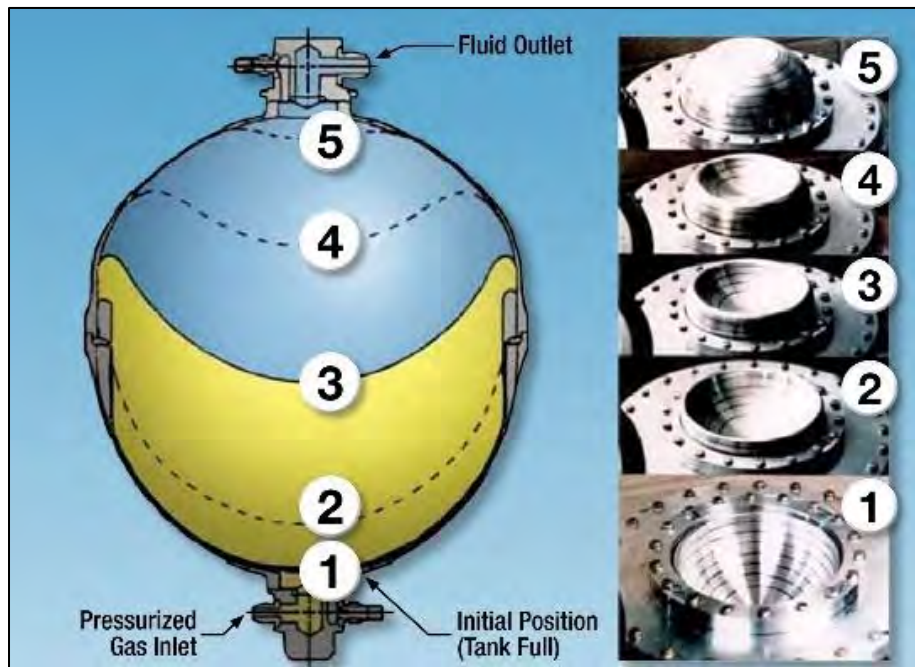


Figure 4-7: Aluminum Rolling Diaphragm Example⁴

Figure 4-8 below provides an overview of the entire subsystem, including the associated valves, regulators and sensors.

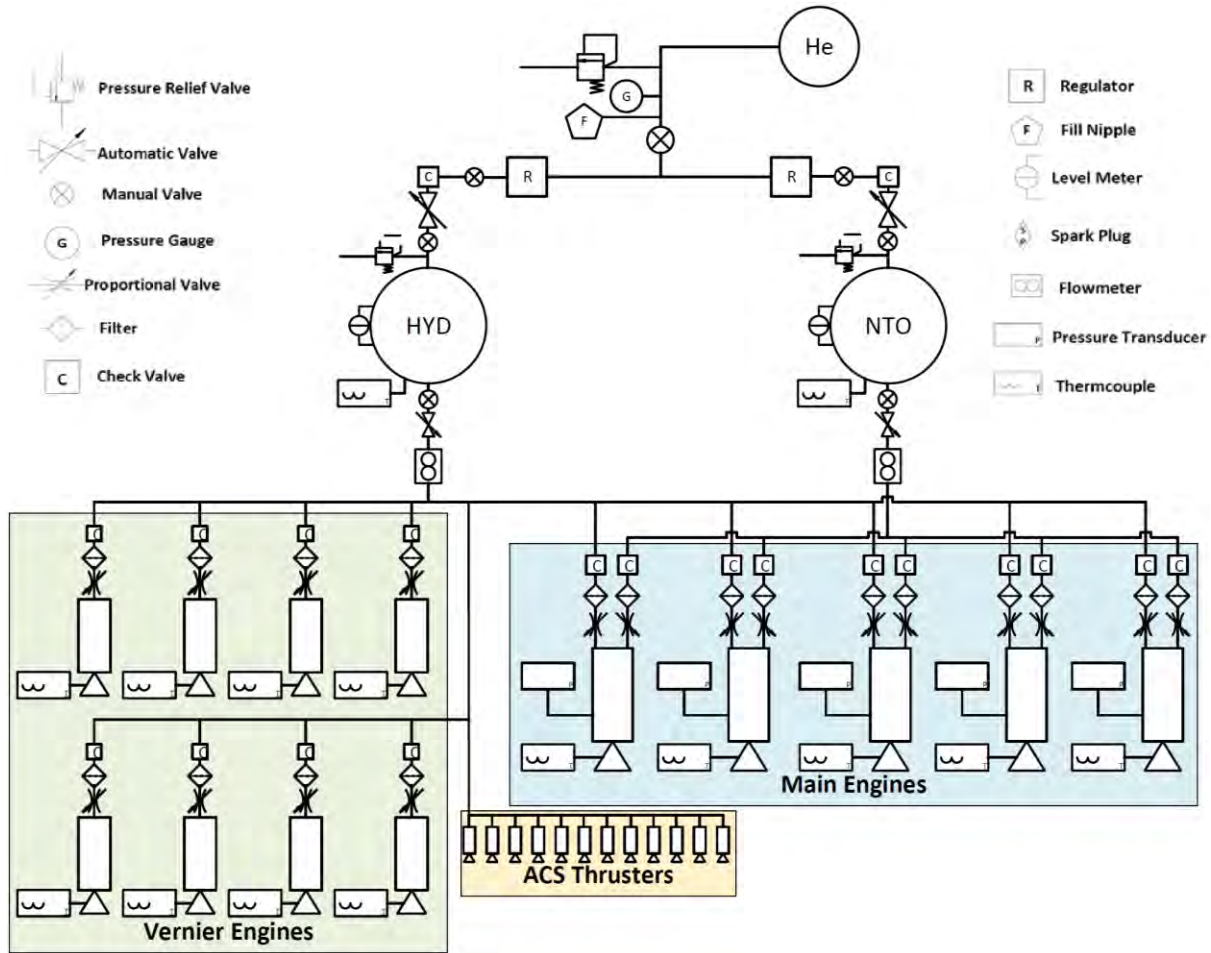


Figure 4-8: Propulsion Subsystem Schematic

4.2.8 Propulsion Mass and Power Statement

The final mass of the propulsion system is 131.6 kg when dry and roughly 1394 kg when wet. The exact value depends on the lander, though the variation between the two is about 10 kg. An itemized breakdown of the subsystem's components can be found on Table 4-8. The subsystem consumes 350 W when firing the main engines and 232 W when firing the required four of the eight Vernier thrusters. It should be noted that these power draws are intermittent, and that the main engines will never be firing at the same time as the Vernier engines. The additional power consumption stems from the heaters for each engine, approximately 13 W per thruster. Table 4-9 details the power consumption for each component, with the total value reflecting that of a system in which every engine is firing.



Table 4-8: Propulsion Subsystem Mass Statement

MASS STATEMENT PER LANDER			
Item	Mass		Notes / source
Propellant	1256	kg	
Pressurant	6.4	kg	
4000 N Engine	34.0	kg	Aerojet R-40B
445 N Thruster	12.8	kg	MONARC-445
Lines and fittings	5.0	kg	Brown Table 4.10
Diaphragms	17.0	kg	Brown Table 4.10
Valves	21.7	kg	Brown Table 4.10
Temp. Transducers	1.5	kg	Brown Table 4.10
Pres. Transducers	1.5	kg	Brown Table 4.10
Fasteners	14.0	kg	Brown Table 4.10
Heaters	22.1	kg	Brown Table 4.10
Margin	2.0	kg	
DRY TOTAL	131.6	kg	
WET TOTAL	1394.0	kg	

Table 4-9: Propulsion Subsystem Power Statement

POWER STATEMENT PER LANDER			
Item	Power		Notes / source
4000 N Engine	350.0	W	Aerojet R-40B
445 N Thruster	464.0	W	MONARC-445
Heaters	169.0	W	Aerojet
TOTAL	983.0	W	

4.3 Power

Driving requirements for the power system are shown in Table 4-10 below.

Table 4-10: Power System Driving Requirements

Req. No.	Requirement Text
4.3.1	Power system shall provide power for all modes of operation
4.3.2	Power System shall provide power for 15 days of science operations
4.3.3	Power system shall provide power in event of mission stoppage



Figure 4-8 shows that two possible power system sources will be RTGs and fuel cells. From this a trade study was conducted to determine the best power source. The results are summarized in Table 4-11

Table 4-11: Power System Trade Study

Requirements	Fulfills? Y/N		
	SA+Batteries	SA+Fuel Cells	RTG
Commercially available & practical	Y	Y	N
Provides power for 30 Day eclipse time	N	Y	Y
Can supply equivalent current at 28V	Y	Y	Y
Provides power in event of mission stoppage	Y	Y	Y
All Requirements Fulfilled?	N	Y	N

The batteries failed because they were impractical for a 30 day mission. The RTG failed because all available stocks are earmarked for current missions and the price tag of 110 million dollars would use too much of the budget.⁵ Further RTGs have a toxic political history and other costs that are hard to predict like environmental lawsuits. Given these factors fuel cell emerged as best choice. Solar panels were added to the fuel cell system if the craft experiences a mission stoppage in space. Two strings of LiPo cells were also added to give eclipse period power for a parking orbit. This set up mitigates against the risk of being in orbit too long and running out of fuel for the FC stack.

4.3.1 Lander Fuel Cell Sizing

The fuel cells chosen are based on the newest proton membrane exchange cells (PEM) developed by Toyota. They offer energy densities 2.2 times greater than other PEM systems⁶. This is accomplished through a 3-D mesh allowing for more reactants per cell. Characteristics of the fuel cells are seen in Table 4-12. Another advantage of these cells is that their operation temperatures are close to the limits of the electronics which simplifies the heating and cooling issues.



Table 4-12: Fuel Cell Characteristics⁷

Cell Voltage	0.67	V
Current Density	1.9	A/cm ²
Power Density	1295	mw/cm ²
Stack Pressure	2.5	atm
Peak cell temp	86	C
Operational temps	60	C
Q/DeltaT	2.5	kW/C
Power per Cell	160	W
# Cells series	42	
Total Stack Power	6705	W

Figure 4-9: Fuel Cell Types and Operating Parameters shows the characteristics, advantages, and disadvantages of various fuel cell types. PEMs were chosen because of their operation temperatures, quick start times, and energy densities. The fuel cell stack was designed with two redundant systems. Each stack is able of powering the lander independently. Each stack consists of 42 cells to meet the voltage requirements. One stack can provide the current demands. Two stacks provide the equivalent of a string out capability for batteries. The specifics of the total system mass are given in Table 4-13



Fuel Cell Type	Common Electrolyte	Operating Temperature	Typical Stack Size	Electrical Efficiency (LHV)	Applications	Advantages	Challenges
Polymer Electrolyte Membrane (PEM)	Perfluorosulfonic acid	<120°C	<1 kW - 100 kW	60% direct H ₂ ⁱ 40% reformed fuel ⁱⁱ	<ul style="list-style-type: none"> Backup power Portable power Distributed generation Transportation Specialty vehicles 	<ul style="list-style-type: none"> Solid electrolyte reduces corrosion & electrolyte management problems Low temperature Quick start-up and load following 	<ul style="list-style-type: none"> Expensive catalysts Sensitive to fuel impurities
Alkaline (AFC)	Aqueous potassium hydroxide soaked in a porous matrix, or alkaline polymer membrane	<100°C	1 - 100 kW	60% ⁱⁱⁱ	<ul style="list-style-type: none"> Military Space Backup power Transportation 	<ul style="list-style-type: none"> Wider range of stable materials allows lower cost components Low temperature Quick start-up 	<ul style="list-style-type: none"> Sensitive to CO₂ in fuel and air Electrolyte management (aqueous) Electrolyte conductivity (polymer)
Phosphoric Acid (PAFC)	Phosphoric acid soaked in a porous matrix or imbibed in a polymer membrane	150 - 200°C	5 - 400 kW, 100 kW module (liquid PAFC); <10 kW (polymer membrane)	40% ^{iv}	<ul style="list-style-type: none"> Distributed generation 	<ul style="list-style-type: none"> Suitable for CHP Increased tolerance to fuel impurities 	<ul style="list-style-type: none"> Expensive catalysts Long start-up time Sulfur sensitivity
Molten Carbonate (MCFC)	Molten lithium, sodium, and/or potassium carbonates, soaked in a porous matrix	600 - 700°C	300 kW - 3 MW, 300 kW module	50% ^v	<ul style="list-style-type: none"> Electric utility Distributed generation 	<ul style="list-style-type: none"> High efficiency Fuel flexibility Suitable for CHP Hybrid/gas turbine cycle 	<ul style="list-style-type: none"> High temperature corrosion and breakdown of cell components Long start-up time Low power density
Solid Oxide (SOFC)	Yttria stabilized zirconia	500 - 1000°C	1 kW - 2 MW	60% ^{vi}	<ul style="list-style-type: none"> Auxiliary power Electric utility Distributed generation 	<ul style="list-style-type: none"> High efficiency Fuel flexibility Solid electrolyte Suitable for CHP Hybrid/gas turbine cycle 	<ul style="list-style-type: none"> High temperature corrosion and breakdown of cell components Long start-up time Limited number of shutdowns

Figure 4-9: Fuel Cell Types and Operating Parameters ⁸



Table 4-13: Power System Specifics

$V_{H_2 \text{ tank}}$	0.05	m^3
$V_{O_2 \text{ tank}}$	0.03	m^3
Reactant Mass	18.98	kg
$m_{\text{outage (1\%)}}$	0.19	kg
$m_{\text{loading-error (0.05\%)}}$	0.09	kg
$m_{\text{Prop-residual (2\%)}}$	0.38	kg
$m_{\text{degradation}}$	4.10	kg
Total Reactant Mass	19.65	kg
m_{H_2}	2.95	kg
m_{O_2}	16.70	kg
$m_{H_2 \text{ tank}}$	71.48	kg
$m_{O_2 \text{ tank}}$	29.57	kg
Lines and fittings	5.00	kg
Pressure Transducers	1.20	kg
Valves	6.84	kg
Fuel Cell Total Mass	142.3	kg
Battery Mass	8.23	kg
Total Power System Mass	150.5	kg

The system is sized for 15 days of maximum power draw at 656 W. The science mission is anticipated to last 10 days, so this gives 5 days of redundancy for the system. Figure 4-10 shows the line schematic of the system. The system consists of composite overwrapped pressure vessels along with the necessary plumbing. Radiators and condensers are used to cool the waste water into liquid form for storage onboard. Inert gas keeps the system at operating pressure and is used to flush the system in the event of a stoppage. Each tank has a feed switch to direct flow to the other stack in the event of failure.

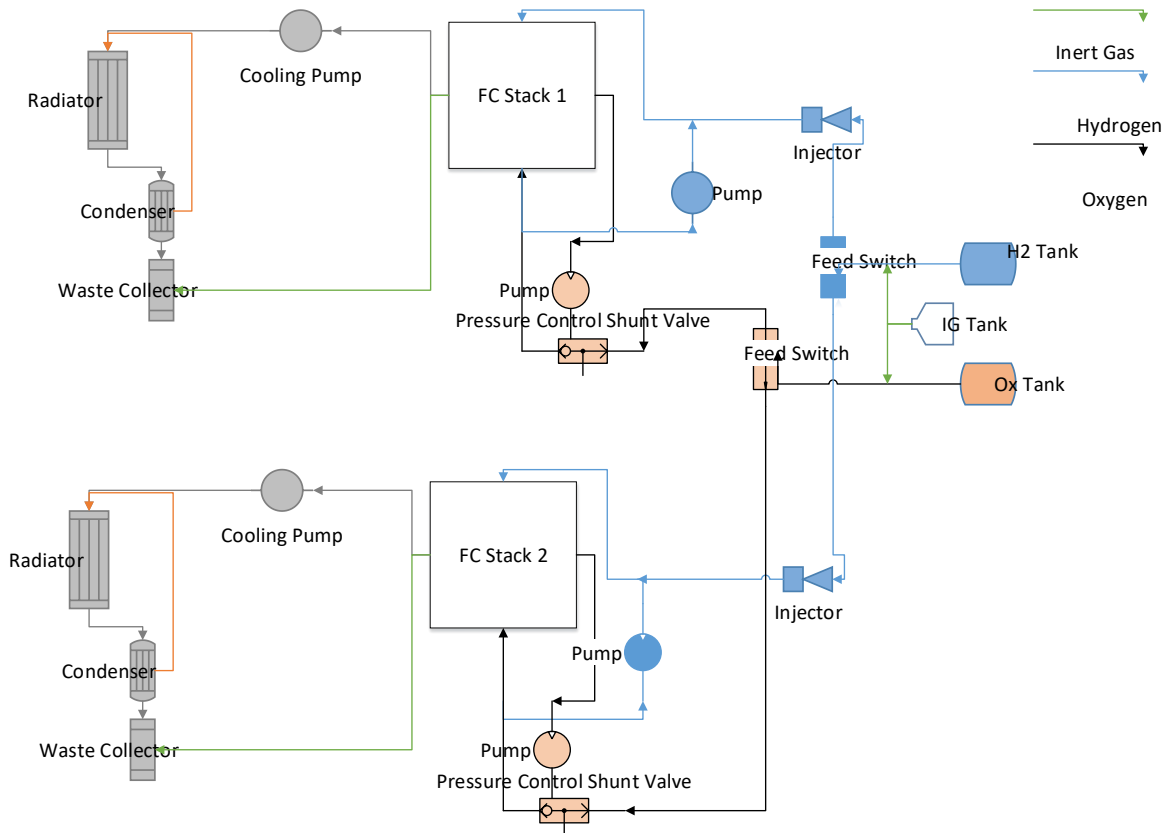


Figure 4-10: Power System Line Diagram

The system is designed with redundant stacks. Each reactant feed system has a feed switch to direct gas flow to the other stack in the event of failure. Each feed line also captures unused reactants and pumps it back into the main line. Water is then extracted via the cooling pump and sent to the radiator and final a condenser that turn any water vapor into liquid where it is stored in the waste collector. An inert gas supply is also used to maintain the stack operating pressuring of 2.5 atm and to flush the system in the event of shut down. The inert gas is also used to pressurize the waste collection tank. In summary the fuel cell system is sized with 5 extra days of power or a 50% margin with redundant components. Given the high-risk environment the landers will operate in this risk mitigation is more than necessary.

4.3.2 Coupler Power System

The coupler system houses the solar panels that provide power to both landers. It also houses the batteries that provide power during eclipse periods of operation. Characteristics of the power system are given in Table 4-14.



Table 4-14: Coupler Power System Characteristic

Cell Voltage	3.70	V
Cell Capacity	10.00	Ah
Cells per string	8.00	
Number of Strings	2.00	
Total Battery Mass	3.36	kg
Solar Array Area	3.28	M ²
Solar Array Mass	66.15	kg
Total Coupler Power System Mass	69.51	kg

The solar arrays can run both landers in their minimum operational mode. The LiPo cells provide power in the event the landers end up in a different orbit. This provides redundancy in case an orbital checkout fails, and the landers have to wait for diagnostics. We can also delay landing by months in case something goes wrong since the fuel cells don't need to be turned on until separation begins.

4.3.3 Power System Mass and Power Statement

The total power budget is given in Table 4-15. Subsystem power allocation was made using Brown's subsystem power allocation guide. Using the other classification Brown gives the following relationship

$$P_t = 210 + 1.3P_{pl}$$

From this based on Brown's power allocation guide the power margin was determined using the BID Class 1 AP category. The full power statement can be seen in Table 4-15. The maximum power demand for each lander is 962 W during full propulsion system power draw, which occurs only during brief periods on the order of minutes. The battery bank and fuel cell output are more than capable of meeting this peak demand.



Table 4-15: Lander Subsystem Power Budget

Subsystem	Allocation, %	Budget, W	Current, W	Status
Thermal Control	33	84	43	C
Attitude Control	11	28	129	C
Power	2	5	5	C
Command & Data	15	38	106	C
Communication	30	76	104	C
Propulsion	4	10	414	C
Mechanisms	5	13	13	E
	Total	255	813	
Margin		229	-330	
Payload		149	149	
Lander On Orbit Power		633	962	
Total SC Power (2x Lander OOP)			1925	

The total power system mass for both landers and coupler system is given in Table 4-16. Mass margin was drastically exceeded because of the redundancy of having two systems and the need for heavy tanks to hold the fuel cells reactants. While the system is heavy there is still over 900 kg of mass margin left over so the heavy power system is acceptable.

Table 4-16: Power System Mass Statement

Total FC mass	142.30	kg
Battery Mass	3.36	kg
Cabling	40.00	kg
Control Equipment		
Power Control Unit	9.03	kg
Power Distribution Unit	4.69	kg
Shunt Regulator	6.02	kg
Signal Processing Unit	1.89	kg
Total Power System Mass	207.3	kg
Solar Array Mass	66.15	kg
Total Power System Mass Two lander	273.44	kg



4.4 Thermal

Driving requirements for the thermal protection system (TPS) are given in Table 4-17 while Table 4-18 shows the thermal limits from Brown⁹.

Table 4-17: Driving Thermal Requirements

#	Requirement Text
1	Thermal Protection System shall allow for operations at maximum power in all flight regimes
2	TPS shall keep electronic within thermal limits
3	TPS shall keep fuel tanks within thermal limits

Table 4-18: Thermal Limits⁹

Item	Lower Temp, K	Upper Temp, K
Electronics	273	313
Hydrazine	280	308
Solar Arrays	173	373
Structures	227	338

Launching into a 300 km orbit is routine for satellites. Even the cruise phase to the Moon is not too challenging of an environment thermally speaking. The real challenge comes in the shaded craters of the Moon. Figure 4-11 shows the flux received in Scott and Noble is almost zero and the ambient temperature is around 40K.

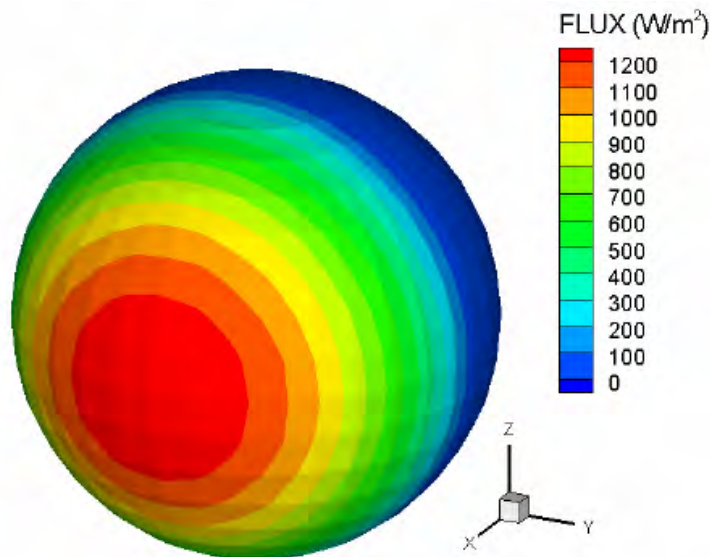


Figure 4-11: Lunar IR Environment ¹⁰



Table 4-19 shows the steady state worst case temperatures for the maximum and minimum power draws of the landers. The major limiters are the electronics and the hydrazine tanks. The upper and lower limits for Hydrazine were used along with a 5 degree K margin per Brown's guidelines⁹. In order to find the temperatures a bulk thermal analysis was done with steady state assumptions.

Table 4-19: Steady State Thermal Properties

Mission Stage	Max Power Dissipation (W)	Min. Power Dissipation (W)	T _{max} (K)	Radiator Area (m ²)	Heater Power (W)
LEO (300 km)	633	316	446.4	0.70	14
LMO (50 km)	633	316	444.5	0.71	10.9
Lunar Ground (0 km) Dark	633	316	317.1	2.76	42.6

The fuel tanks have been thermally isolated using MLI. Figure 4-12 shows how the TPS will operate and what parts it will use. Louvers, radiators, heat pipes, and MLI are used to passively control the temperature of the spacecraft. When the lander begins to warm louvers are used to control how much heat is radiated away. Heat pipes will keep the electronics cool during flight. One on the ground the louvers will lower the emissivity of the radiators keeping the landers warm in the craters. The fuel tanks are covered in MLI to keep them within their thermal limits. Since no heat is being generated internally they will passively radiated heat to the environment. The landers are kept warm using aluminized MLI. Using historical data, it was found 30 layers would give an effective emissivity of 0.05¹¹. Using an outer layer of Kapton with an absorptance of 0.14 will give thermal results consistent with Table 4-19.¹²

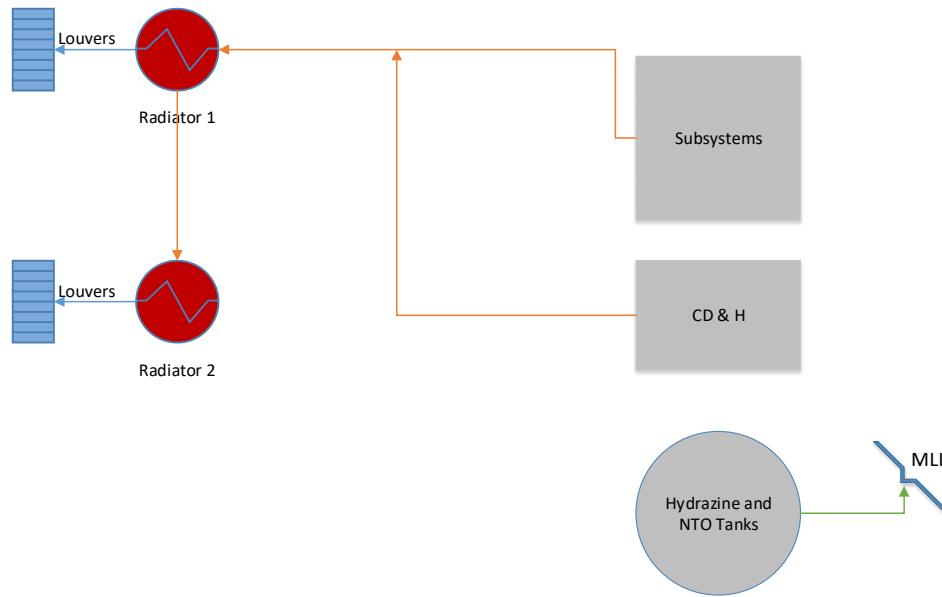


Figure 4-12 Thermal Block Diagram

To better understand the heating that the landers will experience in space, transient heating analysis was done using the STK's Space Environment Effects Tool. Figure 4-13 shows the heating experienced by the landers in a 30-day low Earth orbit with the same parameters as the initial parking orbit. This analysis was done to determine if the craft could survive being in orbit longer than expected if maintenance or extended systems checks were needed. The temperatures fluctuate between 374-380 K which is within the range of temperatures the TPS is designed to handle.

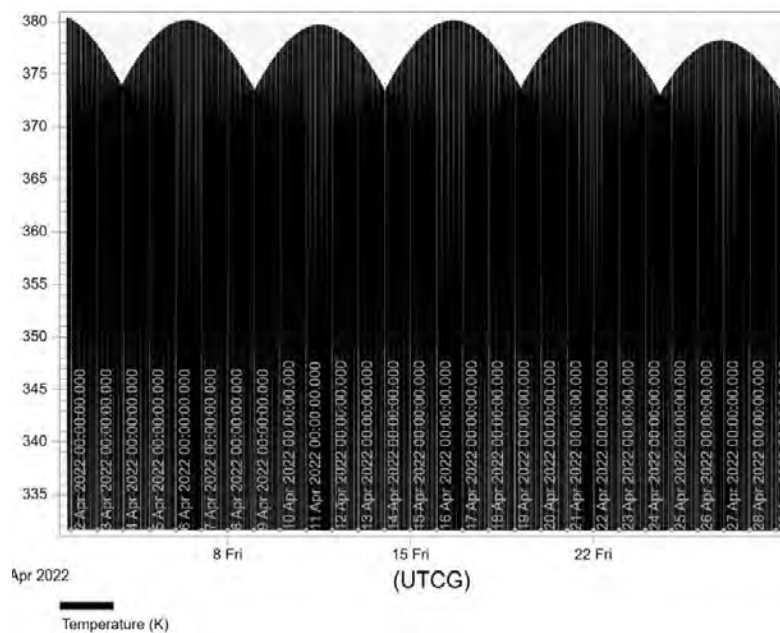


Figure 4-13: Transient Heating of Landers in 30-day LEO orbit



Transient analysis is also shown for the cruise phase. This time since the craft can't cool off in the Earth's shadow the temperature is higher at 419K but not higher than the worst-case results in the steady state analysis. The TPS will be more than capable of handling these temperatures.

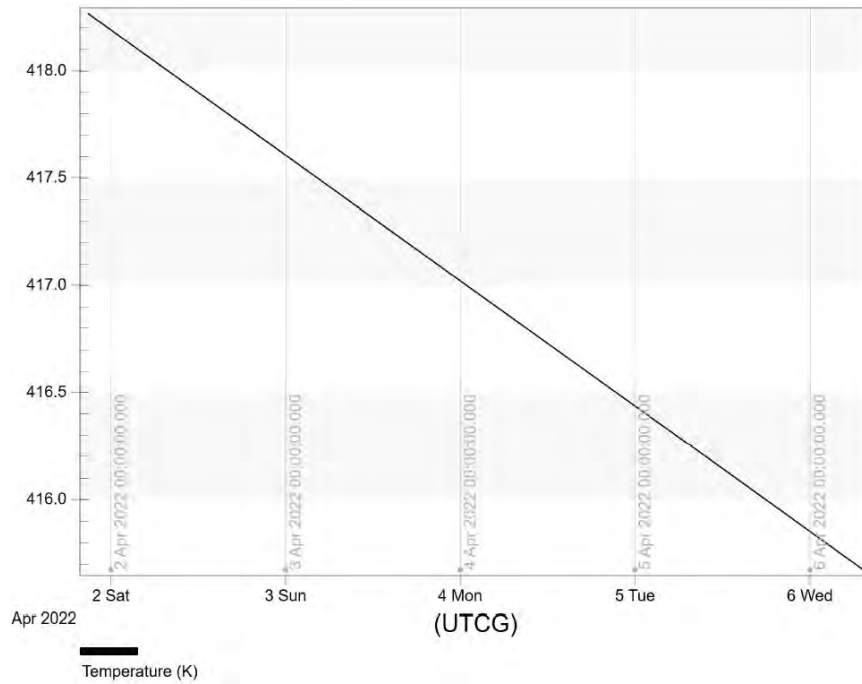


Figure 4-14: Transient Heating of Landers in Transit

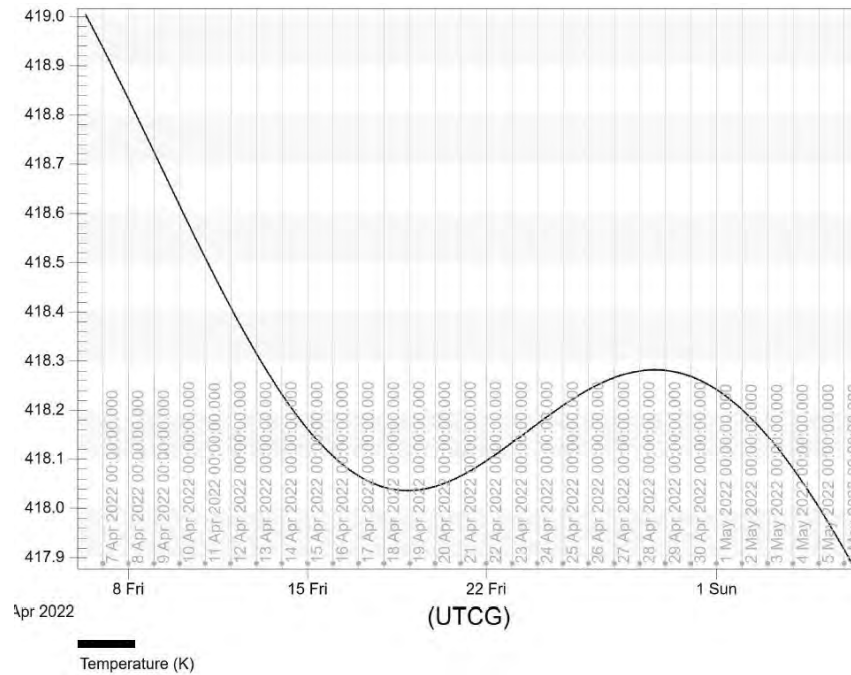


Figure 4-15: Transient Heating in Lunar Orbit



Figure 4-14 shows the transient heating for the Lunar Orbit. Again, these temperatures are below the worst case steady state results, so we can expect the TPS to be able to handle all flight regimes. It is also important to note that in the event the landers must stay in Earth or Lunar orbit longer than expected the batteries and solar panels provide more than enough power to run the TPS system. All transient analysis was done assuming 300W minimum power draw. This is more than enough to run all the subsystems which draw 255W.

4.4.1 Thermal System Mass and Power Statement

The final thermal control statement is given in Table 4-20, using MLI, heat pipes, radiators, and louvers passive thermal control is achieved. Heaters are used to keep some components warm in the crater's cold environment.

Table 4-20: Orbiter Thermal Control Statement

Item	Mass (kg)
Multilayer Insulation	0.72
Heat Pipes	3.3
Louvers	7.3
Thermostats	0.03
Heaters	4
Radiators	1.94
Paint	5.75
Total per Lander	23.0

4.5 Attitude Control System (ACS)

The requirements for the lander's attitude control system are derived from the needs of the architecture design. These requirements are shown in Table 4-21. The first requirement is that the ACS shall be able to provide controlled descent during the landing phases. The second is that the ACS shall be able to allow the landers to avoid potential landing hazards, e.g., lunar boulders.

Table 4-21: Attitude Control System Requirements

#	ACS Requirements
1	Provide controlled descent during the landing phases
2	Allow landers to avoid potential landing hazards (e.g., lunar boulders)



To accomplish these requirements, three different types of attitude control systems were considered. These types were, spin-stabilization, reaction wheel control (RWA), and 3-axis control thrusters. A trade study down-select, shown in Table 4-22, was performed. From this trade study, it was determined that the 3-axis control thrusters is the best option. 12 coupled thrusters are capable of orienting the landers during descent and lateral movement. Spin-stabilization, while great during cruise as it passively controls the spacecraft attitude, it cannot meet either requirement. Reaction wheels could meet the first requirement, but cannot meet the second, and therefore was also ruled out.

Table 4-22: Attitude Control System Down-Select Trade Study

	ACS Req. #1	ACS Req. #2
Spin-Stabilization	X	X
Reaction Wheels	✓	X
3-Axis Control Thrusters	✓	✓

Similar to all components for the attitude control system, the 3-axis control thrusters that were selected for the landers were then down-selected as well. Hydrazine monopropellant thrusters were only considered as they are capable of being pulsed to save fuel, use an identical fuel to the main engine, but most importantly because water is not a byproduct of their chemical reaction, limiting any potential contamination on the landing site. Five different thrusters were considered, the Aerojet MR-103D, Aerojet MR-103G, Aerojet MR-103M, Aerojet MR-111C and the Aerojet MR-111E¹³. The performance characteristics of all these thrusters are shown in Table 4-23. The Aerojet MR-111C, shown in Figure 4-16, was selected for its higher thrust output, which is needed to orient and laterally maneuver the spacecrafts during landing, discussed further in 4.5.3.

Table 4-23: Attitude Control Thruster Down-Select Trade Study¹³

Model	Thrust (N)	Mass (kg)	Power (W)	I _{sp} (s)
Aerojet MR-103D	1.02	0.33	8.25	224
Aerojet MR-103G	1.13	0.33	8.25	224
Aerojet MR-103M	0.99	0.16	7.1	221
Aerojet MR-111C	5.3	0.33	8.25	229
Aerojet MR-111E	2.2	0.33	8.25	224



Figure 4-16: Picture of Selected ACS Thruster, the Aerojet MR-111C (Courtesy of Aerojet)

4.5.1 System Response Curves

The effectiveness of the selected Aerojet MR-111C was assessed before the down-select. Using the parameters of the thruster, the approximate lander mass, and the moments of inertia, as measured by the lander CAD model, the thruster's performance in orienting and laterally maneuvering the landers was determined. A summary plot of the Aerojet MR-111C's capability in rotating the landers in a 60 second window is shown in Figure 4-17. Due to the symmetry of the lander, the curve for θ_x is identical to that of θ_y and is therefore hidden behind its curve. And for lateral displacement, a summary plot of the selected thruster's capability in a two minute window is shown in Figure 4-18. Because the length of each hop is two and a half minutes, two minutes was selected for this benchmark to show the capabilities in a margined time window.

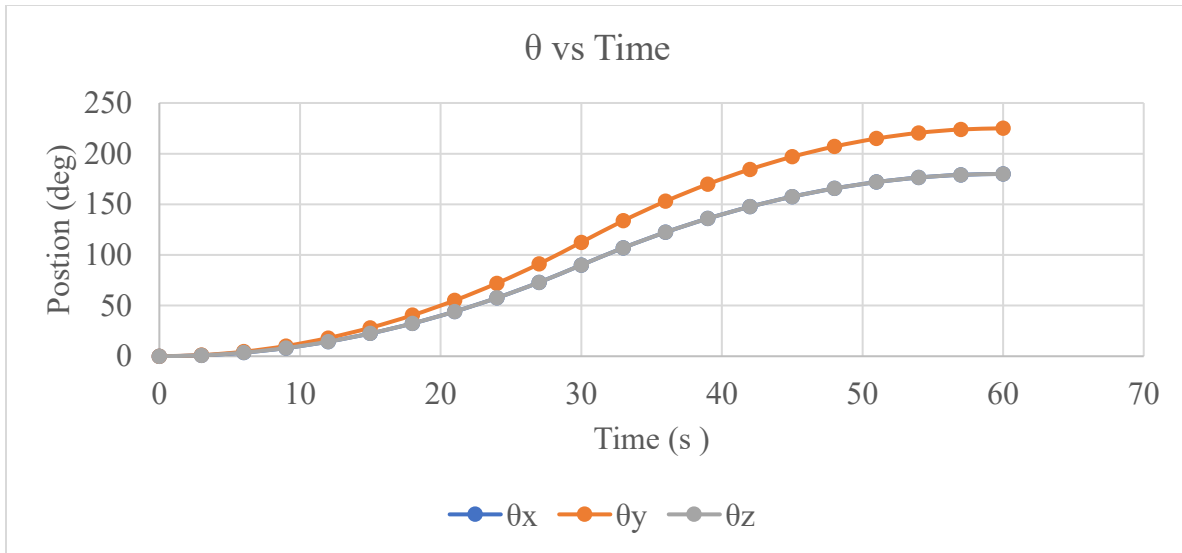


Figure 4-17: Aerojet MR-111C's capability to rotate a lander in a 60 second window

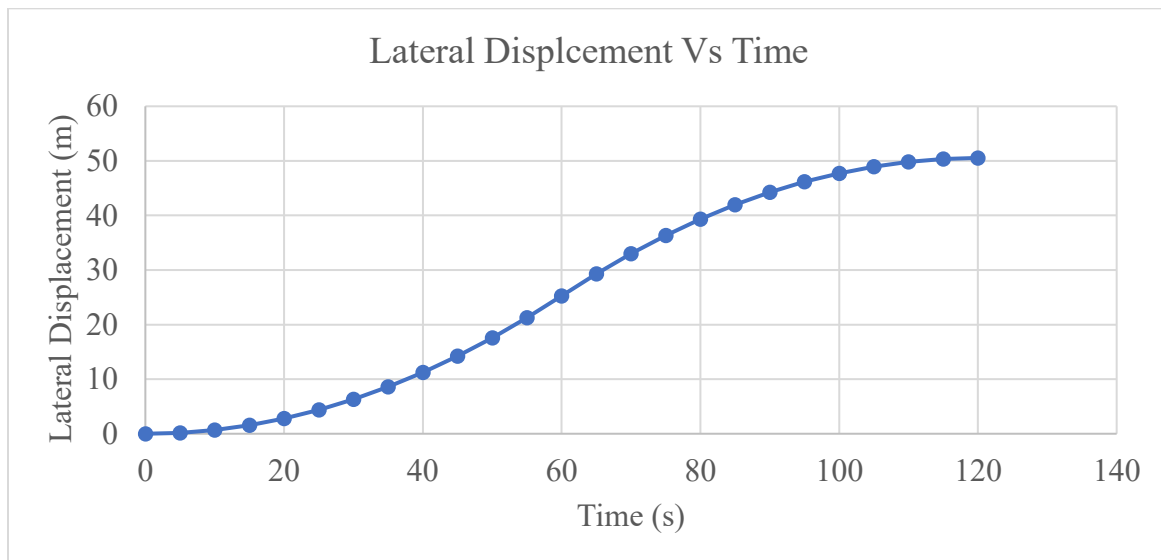


Figure 4-18: Aerojet MR-111C's capability to laterally move a lander in a 2 minute window

4.5.2 Fuel Consumption Analysis

To size the propellant needed for the ACS, the fuel used during the landing sequences, the lateral movement during each hop, and the fuel needed to counteract orbital disturbances needed to be calculated.

For the duration of the landing sequence, 500 seconds, it was conservatively assumed that average of 4 ACS thrusters will be in operation at a given moment. With this assumption and using the mass flow of the Aerojet MR-111C, the amount of propellant needed for landing was calculated to be 5.6 kg.



For the lateral movement during a hop, again, it was assumed that an average of 4 thrusters will be in operation at a moment. As stated in 4.5.1, in 2 minutes, the ACS is capable of moving the lander 50 m, which is puts the lander outside the water plume created by the main engine on the ascent of the hop. Using this 2 minutes as the operation time per hop, the propellant needed for all hops was calculated to be 33.3 kg.

Lastly, the fuel needed to counteract orbital disturbances was calculated. The orbital disturbances assessed were the solar pressure torque, atmospheric drag while in LEO, the gravity gradient torque while in LEO, and the magnetic torque while in LEO. A summary of the torques these disturbances place on the spacecraft are shown in Table 4-24. With these torques, and the duration the landers remain in LEO and LLO, the ACS fuel needed was calculated to be about 0.5 kg.

Table 4-24: Torques on Landers from Orbital Disturbances

Disturbance	Torque Value (N-m)
Solar Pressure Torque	8.26 E-6
Atmospheric Drag	8.14 E-4
Gravity Gradient	2.08 E-13
Magnetic Torque	5.47 E-5

Shown in Table 4-25 is the total fuel needed for the landing sequence, all hops and for orbital disturbances. To confident that the ACS has enough fuel for the mission life, a possible extended mission, and for fault mitigation needs, a contingency factor of 2 was applied to the cumulative propellant mass for the ACS.

Table 4-25: Summation of all Propellant Mass needed by Mission Phase

Mission Phase	Propellant Mass (kg)
Landing Sequence	6.0
Lateral Hops	33.4
Orbital Disturbances	0.5
CUMULATIVE w/ factor of 2x	79.6



4.5.3 Landing Accuracy

To make sure each lander safely arrives at its landing site, a rich set of ancillary equipment was added to the attitude control system. This equipment includes star-trackers, sun sensors, inertial measurement units, and LiDAR system. Further, to make sure the selected equipment for these items most fit the mission needs, a trade study down-select was done for each.

The attached star-trackers and sun sensors allow the spacecraft’s position and attitude while in cruise to be determined. In order to accurately determine the spacecraft’s position and orientation while in cruise, two reference points are needed. These two units are needed so that the location of the spacecraft can be tracked and monitored until its descent onto the lunar surface, by finding the fixed reference point to the stars and sun, respectively. The considered star trackers for the ACS are shown in Table 4-26, and the considered sun sensors are shown in Table 4-27. Ultimately, the Vectronic VST-41M star tracker was chosen because of its increased accuracy over the other options, while remaining relatively light at 0.9 kg. This accuracy was desired due to the precision needed to accurately land at the desired landing site. Although only 3 star trackers are needed, a fourth is added as a backup. Similar to the star tracker, the Adcole Spinning Sun sensor was selected for its greater performance, including adding a fourth for redundancy. The power provided by the fuel cells allows for the unit’s wattage, so the performance increase was taken.

Table 4-26: Trade Study Down-Select for ACS Star Tracker^{14, 15, 16}

Star Tracker	Mass (kg)	Power (W)
Terma T-2	0.45	2.5
Ball CT-2020	3	8
Vectronic VST-41M	0.9	2.5

Table 4-27: Trade Study Down-Select for ACS Sun Sensor^{17, 18}

Sun Sensor	Mass (kg)	Power (W)
Adcole Spinning Sun Sensor ($\pm 64^\circ$)	0.110	0.4
Solar Mems SSOC-D60	0.035	0.35
Solar Mems SSOC-A60	0.0275	0.036

To determine the translational velocity and rotational velocity of the landers during the landing and hopping phases, inertial measurement units (IMU) are utilized. The ACS uses the data generated by the IMU to correct any rotations that offset the landers during landing via a feedback control loop. A summary of the IMUs are considered



are shown in Table 4-28. The Honeywell HG1700 was selected over the other options for its increased accuracy. For redundancy, a second HG1700 was added to the system, to account for the potential failure of one.

Table 4-28: Trade Study Down-Select for ACS Inertial Measurement Unit^{19, 20, 21}

IMU	Mass (kg)	Power (W)
Northrop Grumman LN-200S	0.8	12
ATA IMU	1.5	15
Honeywell HG1700	0.9	5

The last item added to the ACS was a LiDAR unit to track the lander's altitude during descent, and to determine the terrain of the landing site. To achieve this, the Morpheus mission's autonomous Landing Hazard Avoidance Technology (ALHAT) was used. ALHAT has the characteristics shown in Table 4-29. Each lander's altitude needs to be determined so that the ACS and Propulsion subsystem Vernier engines can alter the thrust so that they land softly on the lunar surface via a feedback control loop.

Table 4-29: ALHAT Performance Characteristics

Parameter	Capability
Max Op. Range	50 km in atm., 4000 km w/out atm
Resolution	0.5m at 20 km
Precision	5 cm
Data Update Rate	30 Hz
Operational Wavelength	1.57 micron
Dimensions	10.25" x 8.75" x 6.5"
Mass	10.9 kg
Power	70 W

4.5.4 ACS Mass and Power Statement

Below, in Table 4-30, is the summary of all equipment used in the attitude control system for each lander. Of note, while the mass of the thrusters is sized to all 12 thrusters in the system, the power is only for 4 thrusters. This decision was made, as in no situation would all 12 thrusters would be firing during nominal operation, and 4 was deemed an effective design point.



Table 4-30: Attitude Control System Mass and Power Statement

	Mass (kg)	Power (W)
12x Thrusters	4.0	33
Propellant	79.6	0
Star-Tracker	3.6	10
Coarse Sun Sensor	0.4	2
IMU	1.8	10
LiDAR (ALHAT)	10.9	70
Totals	100.3	125

4.6 Telecommunications

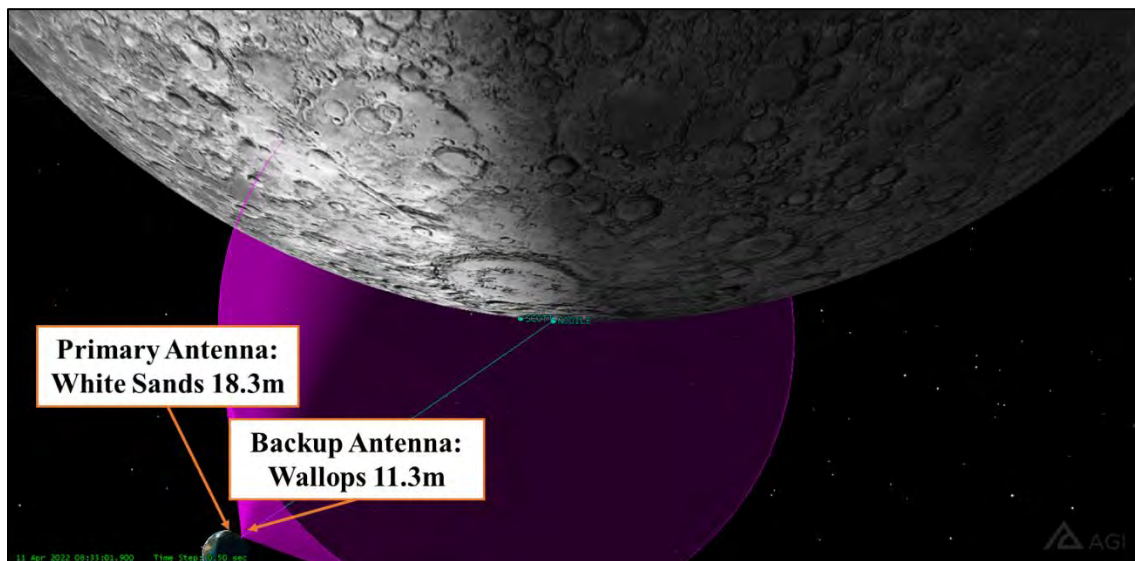


Figure 4-19: Landing Site Access Diagram

As previously mentioned, the access window for this mission is a difficult challenge to overcome. The possibility of a relay satellite was investigated over the course of the design, but it became too expensive for the architecture without significantly reducing the amount of data return. DIANA will have to downlink with direct line of sight to the Earth. Given that DIANA will only be able to see out of their craters directly to the Earth for a limited amount of time, all the data gathered must be transmitted during the visibility window. With the priority of data return in mind, the following link budget demonstrates the “absolute maximum” data return rate with acceptable engineering amounts of errors in the returned data.



Table 4-31: Ground Station Link Budgets Important Results

DIANA Downlink to WSGS			DIANA Downlink to Wallops		
Set Freq	2.30	GHz	Set Freq	2.30	GHz
Range	384400	km	Range	384400	km
Data Rate	20	Mbps	Data Rate	20	Mbps
Transmitter Power	5	W	Transmitter Power	5	W
Antenna Diameter	1	m	Antenna Diameter	1	m
Carrier Link Margin	56.7	dB	Carrier Link Margin	52.5	dB
Eb/N0 Achieved	12.3	dB	Eb/N0 Achieved	8.2	dB
Eb/N0 Required	4.5	dB	Eb/N0 Required	4.5	dB
Data Link Margin	7.8	dB	Data Link Margin	3.7	dB

DIANA will communicate over S-band frequencies to be able to connect with both the primary and backup antenna. According to the Near Earth Network (NEN) User's Guide²², using a 2300 MHz communication channel allows for linking with both the White Sands 18.3 m antenna and the Wallops Island 11.3 m antenna.

4.6.1 Primary Ground Station – White Sands 18.3 m

Located in White Sands, New Mexico, the 18.3 meter antenna is primarily a TDRSS ground station. It is designed to handle large volumes of data arriving from the International Space Station that gets routed through TDRSS. The Lunar Reconnaissance Orbiter (LRO) has also used this antenna to downlink data from the Moon. This makes the antenna a prime candidate for DIANA to downlink to.



Figure 4-20: White Sands Antenna (NASA Goddard Space Flight Center)

4.6.2 Backup Ground Station – Wallops 11.3 m

Located in Wallops Island, Virginia, the 11.3 meter antenna is a NEN station capable of receiving large volumes of data from constellations of CubeSats. This makes Wallops another prime candidate for DIANA to link to. In the event of poor weather conditions at White Sands, DIANA will be able to link at the same data rate to Wallops, with a much less forgiving data link margin, however.

4.6.3 Telecommunications Mass and Power Statement

The mass and power of the telecommunication subsystem was calculated to accommodate both S-band ground stations using the recommended values found in *New Space Mission Engineering: The New Space Mission Analysis and Design*²³. Table 4-32 shows the total telecommunication mass and power needs. To account for the possibility of the high gain antenna being damaged, a redundant set of low gain antennas were added to each lander. With the redundant set of low gain antennas, the mission can continue, but will require more time to downlink all generated data.



Table 4-32: Telecommunications Mass and Power Statement

	Unit Mass (kg)	Unit Power (W)	No. of Components
S-Band Transponder	3.5	22	2
S-Band Diplexer	0.2	0	2
S-Band Low Gain Antenna (LGA) Cables	3	0	All
S-Band LGA (turnstyle)	0.4	0	2
S-Band Wideband Transmitter	3.5	30	2
S-Band High Gain Antenna (HGA) Cables	1	0	All
S-Band HGA (Parabolic)	1.5	0	1
CUMULATIVE	20.7	104	N/A
FOR 2 LANDERS	41.4	208	N/A

4.7 Command and Data System (CDS)

DIANA’s command and data system is sized to accommodate all the payload instrument’s data rate needs, all spacecraft subsystem needs, and allow for commandability of the lander from the Ground. To accomplish this, the average payload instrument data rate was approximated from historical data on from their respective reference instrument and mission. These estimated average rates are shown in Table 4-33. To be conservative in these estimations, it was assumed that these rates only included the instrument’s science data and does not include their calibration data and engineering telemetry.

Table 4-33: Estimations of the Payload Instrument’s Average Science Data Rates as Based on Historical Information

Lander Payload Instruments	Average Science Data Rate (bps)
MastCam-L	40,000
LUNDI	20,000
ChemCam	1,500
SAMZER	80,000
Robotic Arm	500
Robotic Arm Cam	20,000
TOTAL	162,000



Based on historical mission development information, it was gleaned that as a project’s design matures, the capabilities of the payload instruments expand. This expansion results in increases in the instrument’s science data output rates. To accommodate this expected data rate increase, as well as to account for the unknown instrument calibration data and engineering telemetry, the subsystem engineering telemetry, and account for the data overhead induced by the CCSDS packetization used track and downlink data to Ground, a JPL- recommend contingency factor of 5x was applied to total estimated average science data rate. With this contingent rate, the expected science mission data volume was then calculated, as shown in Table 4-34.

Table 4-34: Approximation of Total Science Mission Data Volume

Data Generation Rate per Lander	162,000	Bps
Contingency Factor	5	N/A
Contingent Data Gen. Rate per Lander	810,000	Bps
Length of Science Mission (10 Days)	864,000	S
Estimated Science Mission Data Volume	700	Gb

4.7.1 CDS Mass and Power Statement

Using this contingent data generation rate and expected science mission data volume presented in Table 4-34, the masses and power needed for the CDS were calculated using the recommended values in Table 8.18 of Brown’s *Elements of Spacecraft Design*⁹, as shown in Table 4-35. The Bulk Data Storage (BDS) was sized to store 24 hours of continuous contingent data generation, as to accommodate the regular 12 hours closed communication window resulting from the Moon’s rotation.

Table 4-35: Command and Data System Mass and Power Statement⁹

	Mass (kg)	Power (W)
Telecomm, S/C Clock (SCLK), Signal Condition, & CMD Processors	30	20
Computer (only)	2	10
Science Data Processor	15	7
Eng. TLM Processor	10	5
Bulk Data Storage (BDS) [64 Gb Cap.]	16	64
CUMULATIVE TOTALS	73	106



4.8 Structures

The biggest requirements for the structures of the spacecraft is the landing capability and the capability for the structure to withstand the max launch loads as seen from Figure 4-21. The important points of analysis are the legs during landing, and the whether the connection points for the spacecraft will survive during the launch. Some parameters for launch are the max axial and lateral acceleration experienced by the payload which can be found from the Falcon 9 Users Guide as seen in the figure below. The largest loads experienced by the payload is during the launch with the design load factors in the figure below.

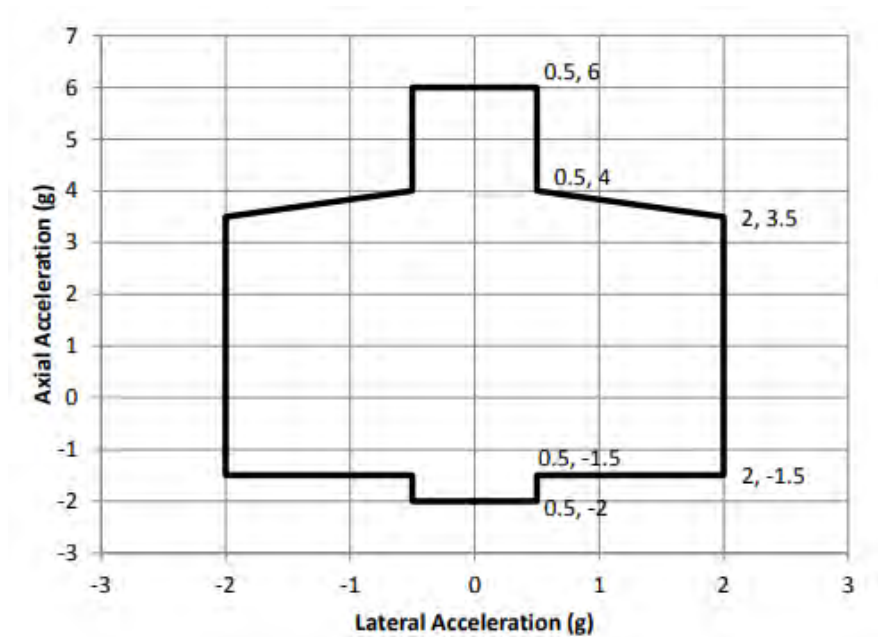


Figure 4-21 Expected Launch Accelerations Given by SpaceX User's Manual²⁴

The above figure is important for the calculations for the spacecraft attachment to the adapter to find the structural integrity of the spacecraft frame as well as the adapters. Worst case load factors were used to calculate stresses for the spacecraft. For the coupler system between the two lander systems, different mass values were used for analysis, as the amount of weight that is pressing down on the coupler will be only one lander and not both landers like the launch vehicle adapter.

The other important factor as previously mentioned is the leg during landing. Things to take note of when doing the analysis is the landing velocity of 1 meters per second which will be changed to 2 meters per second for



innate factor of safety. The landing mass of individual landers. The lander legs will be analyzed assuming the lander will land with one leg which will allow a conservative estimation.

Table 4-36: Aluminum Alloy Trade Study²⁵

Alloy	Formability	Weldability	Machinability	Heat Treatability	Strength
1100	Excellent	Excellent	Good	No	Low
2011	Good	Poor	Excellent	Yes	High
2024	Good	Poor	Fair	Yes	High
3003	Excellent	Excellent	Good	No	Medium
5052	Good	Good	Fair	No	Medium
6061	Good	Good	Good	Yes	Medium
6063	Good	Good	Fair	Yes	Medium
7075	Poor	Poor	Fair	Yes	High

After considering the different kinds of aluminum alloys, shown in Table 4-36, the best choice for our frame is either alloy 6061 or alloy 6063. We chose alloy 6061 as the analysis material because of its good machinability as opposed to 6063's fair machinability. Both alloys have similar material strength, but the 6061 alloy seems to have better machinability out of the two therefore 6061 alloy was chosen as the material choice for the analysis that follows. The idea of using composites was present, but due to their cost we decided to use them on smaller applications such as the shelves for instruments instead of creating the entire frame and legs. The cost of each alloy was kept out because material cost is not as significant as the manufacturing cost which is already implemented in the cost estimation, 5.4 of the proposal.

4.8.1 Launch Vehicle Adapter (LVA) and Coupler Structure

The launch Vehicle Adapter and Coupler will be made from the same type of structure just as seen in Figure 4-22. The launch vehicle adapter will be the RUAG Separation System, while the coupler structure will be made from two payload separation system to attach the two landers at the connection points below and above each spacecraft. This will provide a connection point between the landers for safely securing the two landers and the launch vehicle adapter will be attached to the bottom lander to the launch vehicle to ensure that the entire payload will stay on the

launch vehicle. Detailed information of each component of the interface as well as the coupler structure can be seen in Table 4-37 below.



Figure 4-22: Payload Coupler System Composed of RUAG and the C15 Adapter

Table 4-37: Launch Vehicle Interface and Coupler Structure Specification

System	Description	Mass (kg)	Hardware Specification
Launch Vehicle Interface	Launch Vehicle Adapter	67	C15 w/0.200" wall thickness
	LV-SC Separation System	94	RUAG PAS 702 with 4x 0.75" Explosive Nuts
Coupler Structure	Coupler Adapter	25	C15 w/0.120" wall thickness
	Lander #1 Separation System	94	RUAG PAS 702 with 4x 0.75" Explosive Nuts
	Lander #2 Separation System	94	RUAG PAS 702 with 4x 0.75" Explosive Nuts



4.8.2 Lander Frame Launch Loads - Finite Element Analysis (FEA)

Structural analysis began with calculation of possible extreme load cases for our testing body, which in our case is the spacecraft frame, as well as the landing legs. The spacecraft frame analyzed below using Solidworks implemented the most extreme case of axial acceleration which is 6g and lateral acceleration of 0.5g and multiplied that with the launch mass of 4100 kg. This gave the launch loading on the contact surfaces for the bottom spacecraft frame. As this load case is the worst scenario out of both spacecrafts, doing this analysis would be conservative for the spacecraft frame.

Below, Figure 4-23 demonstrates the load location which is indicated with the purple and brown arrows. This is the spacecraft which is in contact with the launch vehicle through the launch vehicle adapter and the fixture was assumed to be fixed at the top which makes this even more of a conservative analysis.

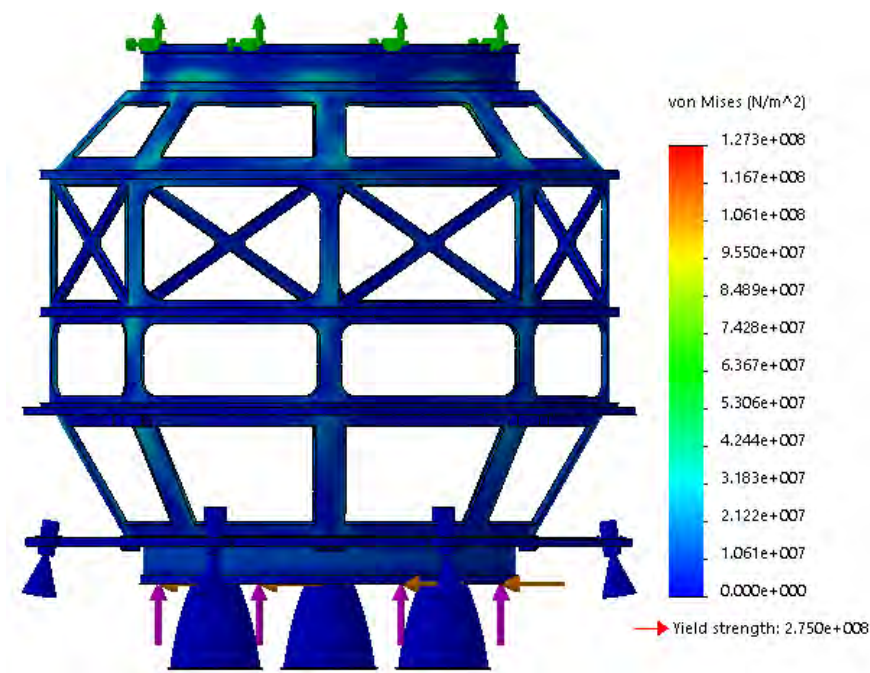


Figure 4-23: Simulation Results for Given Load Case – Side View

As seen above, after the test was run, the structure experienced at max of 127.3 Mpa while the yield strength of aluminum 6061 according to Solidworks is 275 Mpa. This shows that the structure will hold for the load case previously stated. The most stress experienced by the frame is demonstrated at the top of the frame where the angles are most extreme.



4.8.3 Lander Leg Landing - Finite Element Analysis (FEA)

Before the Analysis of the lander legs, some of the parameters that went into the analysis are two meters per second descent velocity, lander initial mass of 800 kilograms, and the conditions were that the entire lander was tilted to one side therefore a single lander leg will take all the loading. This provides a conservative estimation for the legs. The load direction as well as the fixtures applied to the legs are indicated in Figure 4-24 below.

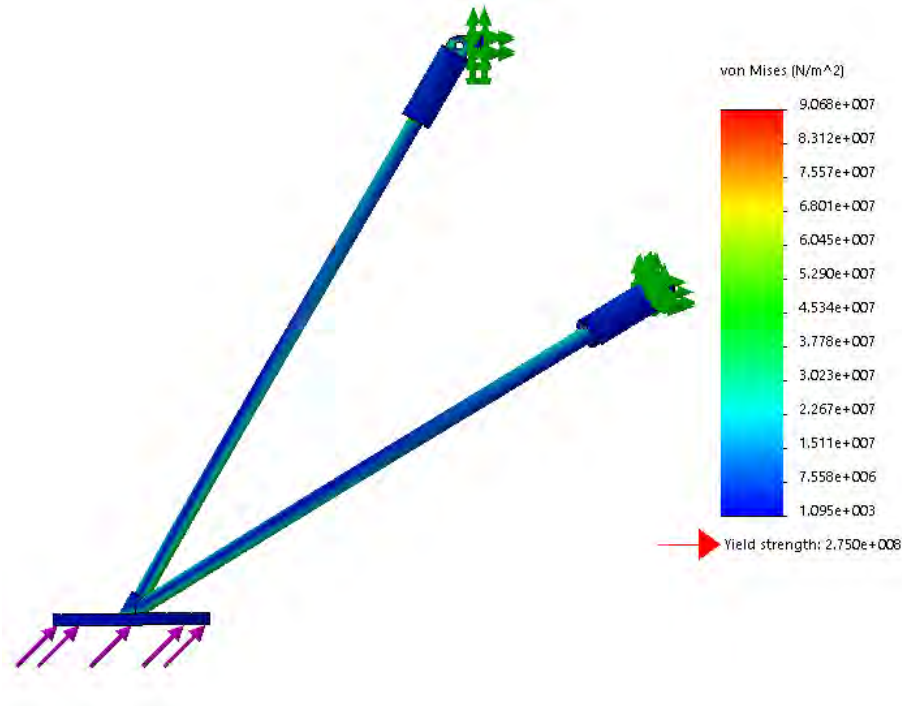


Figure 4-24: Load of 35 kN Lander Leg Analysis Side View

The analysis done above show that the leg will hold. Majority of the legs will not experience any stress when compared to the yield strength. There are certain sharp contours which are fictitious because the dampers at the end of the legs are also analyzed as a single part of the leg. The average loading seen on the leg is actually light green to blue section of the leg which indicate that the leg will survive with the calculated load of 35 kN.

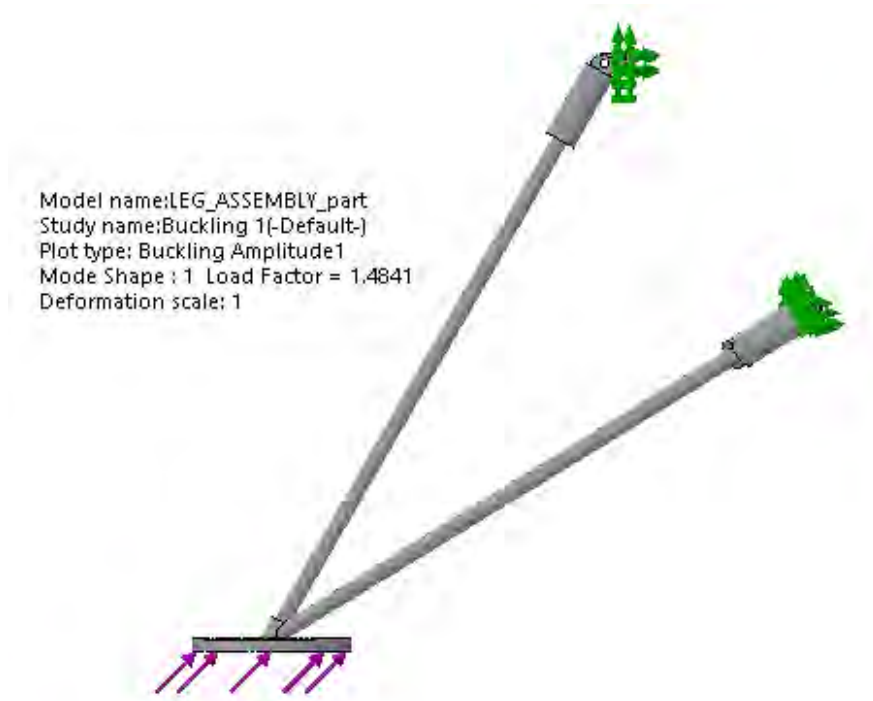


Figure 4-25: Buckling Analysis with Resulting Load Factor of 1.5

Using the buckling analysis tool provided by SOLIDWORKS, we were able to determine that the leg will not buckle under the assumed 35 kN load with a factor of safety of 1.48. This result demonstrates that our preliminary leg design is designed adequately for the expected worst-case loading conditions.

4.8.4 Mechanisms

On our spacecraft, there are various mechanisms that need to be incorporated before it is flight ready. Our Spacecraft will include the use of ordnance devices such as explosive nuts for the separation system between the launch vehicle as well as the staging on the two landers themselves. With the use of ordnance devices, the use of squibs will also be necessary.

Solar panels also require attention, as the two landers are traveling to the lunar orbit, it will have solar panels which keep both landers powered without needing to expend their FC fuel. Solar panels will be held in place by spring loaded hinges which will also be separated with the use of cable cutters which will release the solar panels to their spread-out form during flight. The solar panel's release speed will be controlled by the passive dampers which will also be on board. As for the solar panel articulation, there will be motors present for the rotation of solar panels to reach towards the sun. Cables will be used in tandem with the motors as well as stepper motors to position the solar



panels towards the sun. Note these solar panels are only used during the flight towards the lunar orbit as well as for a short time in the lunar orbit so they do not have to be heavily complicated. A summarized list can be seen below in Table 4-38.

Table 4-38: Summary of Mechanism Table⁹

Mechanisms	Reason for Use
Explosive Nuts	Required for separation system for the LVA as well as the coupler to ensure separation before flight to the lunar orbit and during deployment.
Cable Cutters	Wire cutter ordnance system will be used for holding the solar panels in place until deployed for flight to lunar orbit.
Squibs	Squibs will be used in tandem with explosive nuts and wire cutters to initiate the separation system.
Spring Loaded Hinges	Spring loaded hinges will be necessary to deploy the solar panels to their original spread out position as opposed to its stowed configuration.
Passive Dampers	Passive dampers will be responsible for regulating the speed of deployment of solar panels.
Motors	Motors, such as will be used for solar panel articulation to have the solar panels face the sun during flight and for the duration it is in lunar orbit.



4.9 Fault Analysis and Redundancy

Space is a very harsh environment. As a result, failures of many different types can occur. Below in Table 4-39 the most likely failures for environmental, mechanical, and other effects have been tabled. In Figure 4-26, a risk cube shows the chance and severity of each failure. It should be noted that for many systems with high degree of risk, we have incorporated multiple redundancies for mitigation.

Table 4-39: Summary of Fault Analysis

Failure Number	Description	Consequence	Mitigation
E-1	SA degradation from radiation	Decreased SA performance	Size solar arrays for an EOL capability assuming max radiation degradation for Lunar conditions
E-2	Payload degradation due to single event upset	Partial or full loss of payload	Adequate shielding for payload
E-3	MLI damage from improper application procedure	Thermal damage to SC resulting in full or partial mission loss	Follow NASA MLI application procedure
E-4	EMI interference degrades antenna	Data return rate is lowered	Test SC in model EMI environment
E-5	Thermal environment damages SC	Partial or full mission loss	Thermal vacuum testing to find thermal limits
M-1	SA deployment mechanisms damaged from vibrations	Partial or full mission loss if SA is unable to deploy	20% increase in deployment mechanism mass to resist vibrations
M-2	Valve Failure in fuel stack	Fuel cell can't start resulting in mission failure	Redundant plumbing of fuel system
M-3	Lander legs fail to deploy	Lander crashes resulting in mission loss	Redundant deployment mechanisms
M-4	Fuel cell stack damages from vibrations during launch	Partial or full mission loss if stack is unable to generate power	Vibration isolation for stack
M-5	Mechanical Arm fail to deploy	Partial failure of science mission	Redundant deployment mechanisms
M-6	Landers fail to separate	Mission loss	Redundant separate mechanisms
O-1	Software defects	Partial or full mission loss	Conduct red team software reviews
O-2	Computer failures	System doesn't turn on, deploy, or turns off	Watchdog timers to look for computer problems, safe mode to avoid damage to SC



Probability of Failure

5					
4	E-1		O-2		
3			E-2, M-5	M-4, O-1	
2		M-2	E-3, E-4	E-4, E-5	M-1, M-6
1					M-3
	1	2	3	4	5

Figure 4-26: Fault Analysis Risk Cube



5 Mission Management

5.1 Program Schedule

To keep development on schedule, a programmatic schedule was developed. A summary of this schedule can be seen in Figure 5-1: Program Schedule. With the submittal of this proposal, the project will be already through its preliminary design phase and continuing onto its final design and fabrication phase. Ample time, 2 years is given to the assembly of the spacecraft to accommodate machining of its titanium parts.

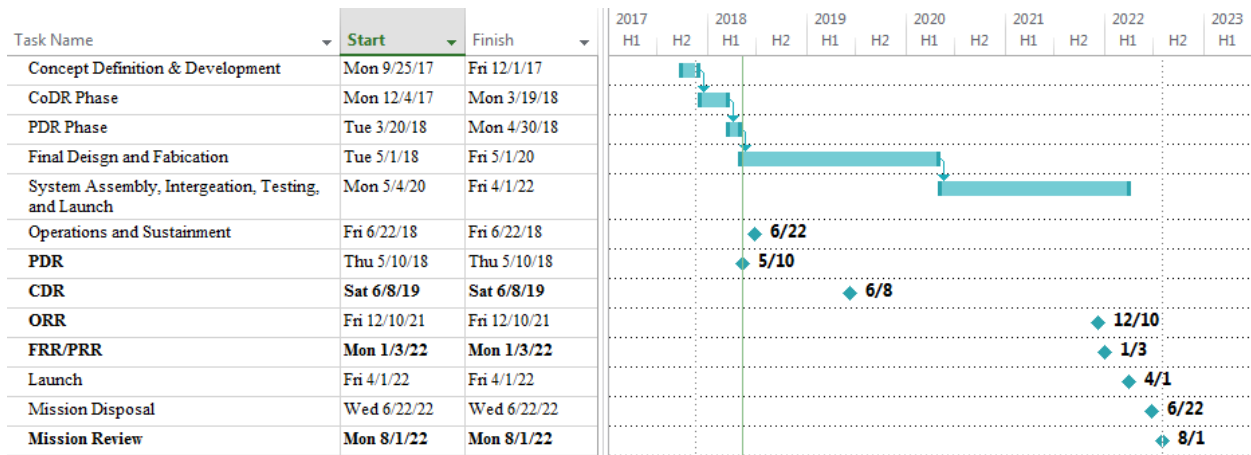


Figure 5-1: Program Schedule

5.2 Manufacturing

Both the spacecraft, DIANA-I and II are expected to be made from aluminum frame primarily the aluminum alloy 6061. Due to its good formability, weldability as well as machinability, difficult sections of the frame can be easily manufactured. The material also helps in its medium levels of yield strength to provide sufficient support during peak stress periods such as launch and landing on the lunar surface. Most parts can be extruded and welded or formed to create necessary parts on the two landers.

DIANA-I and II have been designed in such a way that they are identical, which will aid in manufacturing greatly. The mission profile allows for each lander to complete its portion of the mission with the exact same fuel tanks, thermal components, and communications equipment.



The landers are to be manufactured in tiers to aid in the process as well. The bottom tier contains the legs and the propulsion equipment, the second tier contains the instruments, power, and data equipment, and the third tier contains auxiliary cameras and coupling adapters. The tiers can be seen in Figure 5-2.

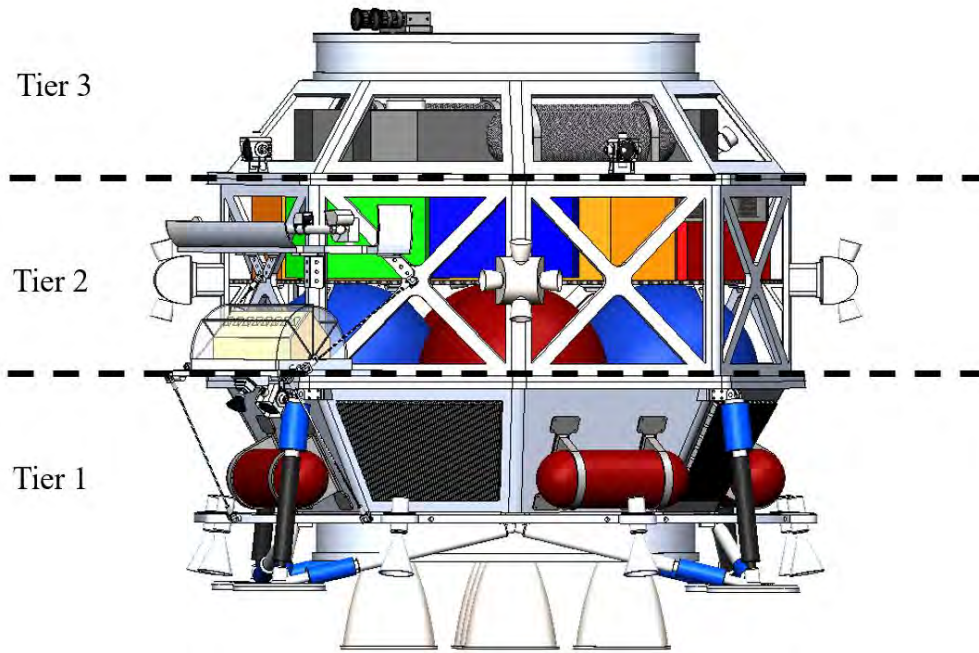
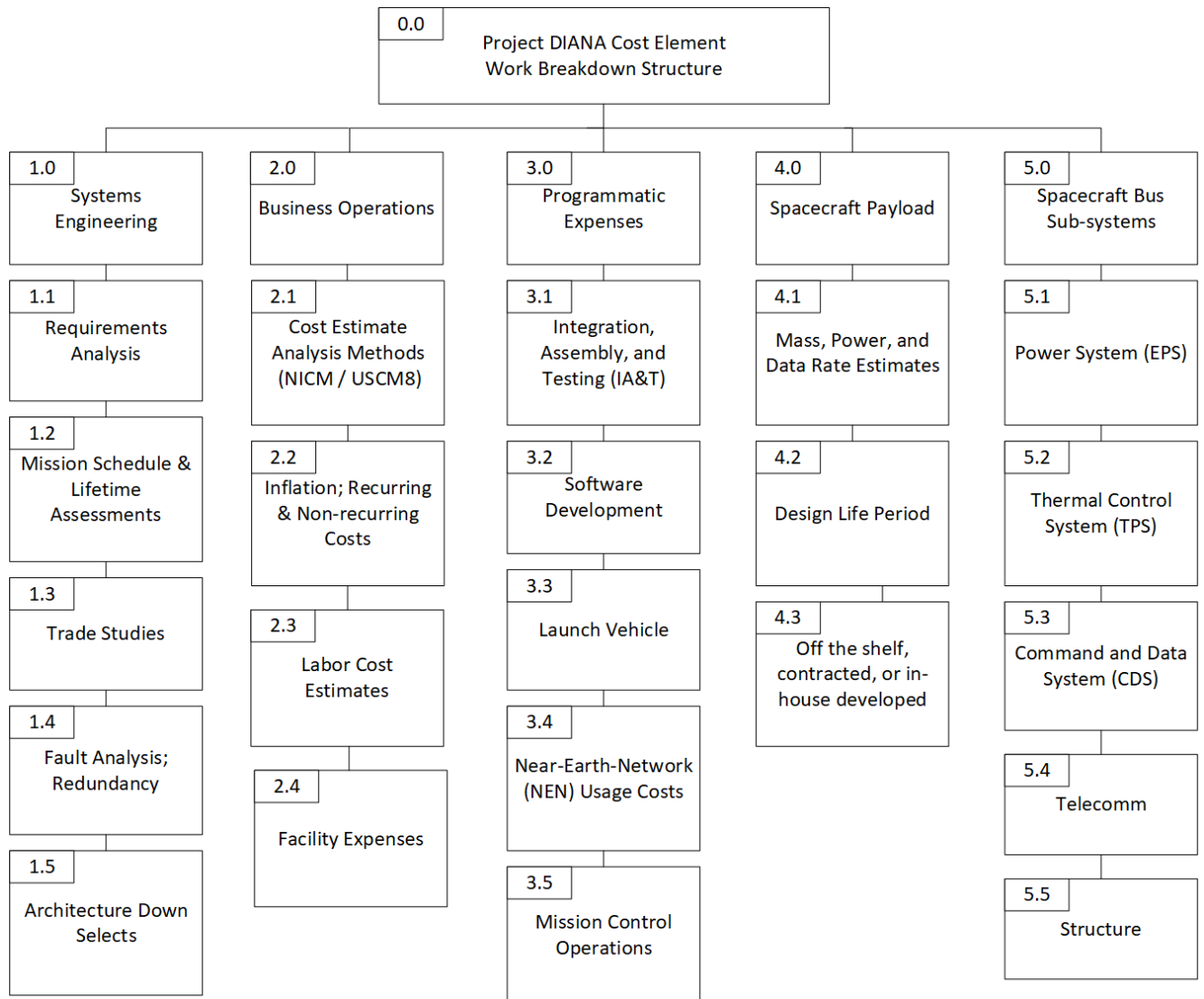


Figure 5-2: Tiered Lander View



5.3 Program Work Breakdown Structure





5.4 Cost Estimates

Cost estimates were performed with the NASA Instrument Cost Model (NICM) for the payload instruments as well as the USAF Unmanned Spacecraft Cost Model (USCM8)²⁶ for programmatic and component cost estimates. By combining these methods, all of the cost elements seen in 5.3 were captured to produce an accurate prediction of mission lifecycle expenses.

Table 5-1: DIANA – I and II Payload Estimation

DIANA – I and II Payload Instrument Costs (Method NICM)			
Payload Instrument	COST DRIVER		COST (\$K) FY2010
MastCam-L	4	kg	2207.5
	45	W	
	0.5	mo	
LUNDI (Lunar Descent Imager)	0.48	kg	683.6
	23.5	W	
	0.5	mo	
Robotic Arm Camera (RAC)	0.6	kg	481.2
	8	W	
	0.5	mo	
Laser Spectrometer (L-SPEC)	7.4	kg	1917
	17	W	
	0.5	mo	
Robotic Arm (RA)	--	kg	1000
	--	W	
	--	mo	
SAMZER (Sample Analyzer)	12	kg	4586.7
	85	W	
	0.5	mo	
TOTAL LANDER PAYLOAD COST [NICM]		\$K	10,876.3
ACTUAL LANDER PAYLOAD COST EST.*		\$M	5.438

Values for the above instruments were taken from the internet, and the cost of each instrument was estimated by using the equation given by the cost model. The instruments were assumed to be half its estimated price because all the instruments were previously used or will be used very soon on different mission.



Lander costs were separated into two different costs, the non-recurring and the recurring costs in which the first developed lander costs more to develop because it's the first model while the second which came after costs less because the process is already set. Detailed cost element breakdowns can be found in Appendix A: Complete Cost Estimate Breakdown. Table 5-2 provides a comprehensive mission cost summary.

Table 5-2: System Cost Compliance Summary

COST COMPLIANCE SUMMARY	
<i>ALL AMOUNTS FOR FY 2017</i>	
METHOD / CATEGORY	\$M
SPACECRAFT COST, NICM + USCM8	411.0
LV: Falcon 9 Full Thrust	62.0
SOFTWARE	12.4
MISSION OPS	6.8
TELECOMM (NEN)	0.6
TOTAL PROGRAM COST, FY17	493
TOTAL BUDGET, FY17	500
COST UNDER BUDGET?	YES
<i>Comparisons:</i>	
Lunar Reconnaissance Orbiter (NASA)	756.0
Mars Science Laboratory (NASA)	2660.0

As we can see in the cost and compliance summary, our lunar prospecting mission system cost is under budget when compared to the total budget of \$500 M in fiscal year 2017.

5.5 Complete Compliance Matrix

Presented in Table 5-3 is the complete compliance matrix for DIANA with respect to the system level requirements set forth in the RFP. The requirement numbering was developed to differentiate the level of the requirements, its type, and its number. The first two numbers are the level, 0 being system level. The next number is type with 0 being science, 1 being programmatic and 2 being budget. The last 3 digits are the ID and start incrementing upwards starting from the number 1.



Table 5-3: Compliance Matrix of all RFP Requirements with Justification

Rq. #	Requirement Text	Met?	Explanation
00.0.001	Mission shall determine the locations and quantities of water deposits in terms of the ratio of water to regolith in two lunar craters.	Yes	Dual lander architecture allows for the exploration of two lunar craters. Robotic Arm & SAMZER allow for in situ measurements of regolith in terms of water composition.
00.0.002	Mission shall discuss the selection of target locations and values of each site; including the assessment criteria.	Yes	The craters, Scott and Nobile, were selected because they are in near permanent darkness, increasing chances of ice, and because the landers have line of sight to the Earth for D/L
00.0.003	Mission shall describe the experiment operations and communication plans.	Yes	Landers' Fuel Cells allow 10 days of continuous operation, with the S-Band HGA capable of downlink to Ground.
00.0.004	Design shall describe sci. approach used in terms of: traceability of specific measurements to sci. obj., planned observations, design of sci. instruments, and collection periods	Yes	Each lander's scientific instruments were each down-selected for their capability to determine the presence of ice most effectively. A logical flow chart of the science operations for each landing site was created.
00.0.005	Mission and design trade studies shall be weighted to prioritize using tech. demonstrated on previous missions or are otherwise in the NASA tech. development portfolio and assessed on the basis of benefit, risk and cost	Yes	All instruments are based off historical missions to minimize cost, complexity and were down-selected based on their capability to effectively determine the presence of ice within the lunar environment.
00.0.006	Mission and design shall demonstrate their fitness at the architecture and system levels through trade studies of: vehicle architecture, launch vehicles, sci. instruments, orbital mechanics, spacecraft subsystem level designs, and other mission level designs	Yes	Trade studies were performed to determine the optimal architecture, launch vehicle, science instruments, orbital trajectories, spacecraft subsystem components and various other mission level designs.
00.1.001	Design shall define mission ops. such as launch, orbit transfer, station keeping as well as other maneuvers.	Yes	Each maneuver necessary to arrive to the moon efficiently and safely are accounted for and down-selected from other trajectories.
00.1.002	Proposal shall be submitted online to AIAA headquarters by May 16, 2018	Yes	The proposal here within was submitted to the AIAA headquarters before the deadline.
00.1.003	Mission shall maximize scientific data return before the end of the mission date of December 31, 2024.	Yes	craters are permanently shadowed craters (where likelihood of water ice presence is highest), & landers explore several locales ea.
00.2.001	Mission architecture and vehicle design shall maximize science data return within cost of \$500 million United States Dollars in FY 2017	Yes	NICM+USCM8 cost estimation method puts total cost under budget



6 Summary Tables

6.1 Spacecraft Mass Statements

E = Estimated

C = Calculated

A = Actual

Table 6-1: Single Lander Mass Statement

SINGLE LANDER MASS STATEMENT			
Subsystem	Budget, kg	Current, kg	Status
Structure	100	164	C
Thermal	15	29	C
ACS	45	102	C
Power	95	207	C
Cabling	30	30	E
Propulsion	65	104	C
CDS	30	73	C
Telecom	30	21	C
LANDER BUS SUB-TOTAL	410	730	
Lander Payload Mass	29	29	C
LANDER DRY MASS TOTAL	500	759	
Propellant	1256	1256	C
Pressurant	7	7	C
LANDER WET MASS	1762	2021	

Table 6-2: Coupler Mass Statement

COUPLER (C) MASS STATEMENT			
Subsystem	Budget, kg	Current, kg	Status
Structure	228	165	A
Thermal	18	9	C
ACS	0	0	A
Power	110	66	C
Cabling	20	20	E
Propulsion	0	0	A
CDS	0	0	A
Telecom	0	0	A
COUPLER MASS TOTAL	376	260	



Table 6-3: Combined Mass Statement Summary

	Budget, kg	Current, kg	Status	Notes
LANDER #1, WET	1762	2021	C+E	Cabling is only remaining estimate
LANDER #2, WET	1762	2021	C+E	Cabling is only remaining estimate
COUPLER W/ SOLAR PANELS	376	260	C+E	Cabling is only remaining estimate
Launch Vehicle Adapter	67	67	A	C29 w/0.200" wall thickness
LV-SC Separation System	94	70	A	RUAG F1663 Payload Separation Ring (PSR)
TOTAL LAUNCH MASS	5400	4439		
<i>Mass Margin</i>		961		

6.2 Spacecraft Power Statement

Table 6-4: Spacecraft Power Statement

Lander Subsystem Power Budget				
Subsystem	Allocation, %	Budget, W	Current, W	Status
Thermal Control	33	84	43	C
Attitude Control	11	28	129	C
Power	2	5	5	C
Command & Data	15	38	106	C
Communication	30	76	104	C
Propulsion	4	10	414	C
Mechanisms	5	13	13	E
	Total	255	813	
Margin		229	-330	
Payload		149	149	
Lander On Orbit Power		633	962	
	Total SC Power (2x Lander OOP)		1925	

The coupler is a net power producer due to its solar arrays and provides 324 W of power to the landers during transit to the Moon. At maximum fuel consumption, the fuel cells can generate 6000 W of power, which is more than adequate to meet peak draw periods during engine burns.



Appendix A: Complete Cost Estimate Breakdown

COUPLER COSTS, NON-RECURRING			
Category	COST DRIVER		COST (\$K) FY2010
Structure + Thermal	174	kg	22,018
Attitude Determination and Control	-	kg	-
Electrical Power System (EPS)	66	kg	4,254
Propulsion	-	cc	-
Telemetry, Tracking, and Command	-	\$K	-
Communications [Telecomm]	-	kg	-
COUPLER BUS COST, NON-RECURRING		\$K	26,271

LANDER NON-RECURRING COSTS (USCM8)			
Category	COST DRIVER		COST (\$K) FY2010
Structure + Thermal	192	kg	23,540
Attitude Determination and Control	23	kg	7,554
Electrical Power System (EPS)	207	kg	13,329
Propulsion	1,112,793	cc	17,121
Telemetry, Tracking, and Command	26,916	\$K	26,916
Communications [Telecomm]	21	kg	12,793
COUPLER BUS COST, NON-RECURRING		\$K	26,271
LANDER BUS COST, NON-RECURRING		\$K	101,252
LANDER [BUS+PAYLOAD + COUPLER] COST, NON-RECURRING		\$K	132,961
IA&T		\$K	25,927
Program Level [Other]		\$K	65,780
Aerospace Ground Equipment [AGE]		\$K	35,610
LANDER COST, NON-RECURRING, FY2010		\$K	260,279
LANDER COST, NON-RECURRING, FY2017		\$M	322



LANDER RECURRING COSTS (USCM8)			
Category	COST DRIVER		COST (\$K) FY2010
Structure + Thermal	192	kg	4,336
Attitude Determination and Control	23	kg	5,145
Electrical Power System (EPS)	207	kg	6,716
Propulsion	1,112,793	cc	8,561
Telemetry, Tracking, and Command	73	kg	7,264
Communications [Telecomm]	21	kg	3,912
LANDER BUS COST, RECURRING			\$K 35,934
LANDER (BUS+PAYLOAD) COST, RECURRING			\$K 41,373
IA&T	-	\$K	5,130
Program Level [Other]	-	\$K	19,252
Launch Operations & Orbital Support (LOOS)	5,850.00	\$K	5,850
LANDER COST, RECURRING, FY2010			\$K 71,605
TOTAL LANDER COST (NON-RECURRING + RECURRING), FY 2010			\$K 331,884
TOTAL LANDER + COUPLER COST, FY 2017			\$M 411

SOFTWARE				
Lines of Code (LOC)			Cost (\$M)	Assumptions
LOP	0.5	M	10	\$20/LOC
TOTAL SOFTWARE COST (FY10)			10.0	
TOTAL SOFTWARE COST (FY17)			12.4	

MISSION OPS			
	Quantity	Annual Cost (\$K)	Total Annual Cost (\$K)
Engineers	7	100	700
Technicians	4	100	400
TOTAL LABOR / YR			1100
MISSION LABOR COST (FY10)			5500
MISSION LABOR COST (FY17)			6810
MISSION LABOR COST (FY17), \$M			6.8
TELECOMM COSTS			
RB	1057	Hourly rate	
AW	0.8	Aperture weighting (HSB station)	
FC	7	Number of station contacts per week	
	364	Number of hours use per year	
AF	1352.96	Aperture fee / hour	
NEN ANNUAL COST (FY09)		492477	\$
		0.49	\$M
NEN ANNUAL COST (FY17)		0.61	\$M
NEN TOTAL COST (5 YR)		3.05	\$M



References

- ¹ “Diviner Lunar Radiometer Observations of Cold Traps in the Moon’s South Polar Region”, Paige, David A., Siegler, Matthew A., et al.
- ² Petro N. E., Mazzarico E., Sun X., Abshire J., Neumann G., Lucey P. (2018). MiLuv Does It Good – The Mini Lunar Volatiles Mission: A Planetary Science Deep Space Smallsat Study of a Lunar Orbiting Mission, 49th Lunar and Planetary Science Conference 2018
- ³ Moog Inc. (n.d.). Spacecraft Propulsion Components - Thrusters. Retrieved from <http://www.moog.com/products/propulsion-controls/spacecraft/spacecraft-propulsion-components/thrusters.html>
- ⁴ M. (2013). Rolling Diaphragm Tanks. Retrieved from http://www.moog.com/content/dam/moog/literature/Space_Defense/Spacecraft/Propulsion/Rolling_Diaphragm_Tanks_Rev_1013.pdf
- ⁵ NASA. (2013). *Multi-Mission Radioisotope Thermoelectric Generator*. Washington, DC.
- ⁶ Yoshida, Toshihiko, and Koichi Kojima. "Toyota MIRAI fuel cell vehicle and progress toward a future hydrogen society." *The Electrochemical Society Interface* 24.2 (2015): 45-49.
- ⁷ Department of Energy. Hydrogen Fuel Cells. Retrieved from https://www.hydrogen.energy.gov/pdfs/review17/fc163_james_2017_o.pdf
- ⁸ Department of Energy. Fuel Cells Comparison. Retrieved from <https://www.energy.gov/eere/fuelcells/comparison-fuel-cell-technologies>
- ⁹ Brown, Charles D. *Elements of Spacecraft Design*. American Institute of Aeronautics and Astronautics, Inc., 2002.
- ¹⁰ Mastropietro, A.J., et al. *Lunar Reconnaissance Orbiter (LRO) Thermal Design Drivers and Current Thermal Design Concept*. NASA Goddard, 2005, *Lunar Reconnaissance Orbiter (LRO) Thermal Design Drivers and Current Thermal Design Concept*, tfaws.nasa.gov/TFAWS05/Website/files/ThermalPaperSession/tfaws_2005_mastropietro.pdf.
- ¹¹ University of Maryland. (2013). *Thermal Analysis and Design*, College Park, MD.
- ¹² NASA. (1999). *Multilayer Insulation Material Guidelines*. Washington, DC
- ¹³ Aerojet. (2006). *Monopropellant Rocket Engines*[Brochure]. Redmond, WA.
- ¹⁴ Terma. (2012). *T1 & T2 Star Trackers: Miniaturized Optical Heads & Electronic Unit*[Brochure].
- ¹⁵ Ball (2018). *CT-2020*[Brochure].
- ¹⁶ Star Tracker VST-41M. (n.d.). Retrieved from <https://www.vectronic-aerospace.com/space-applications/star-sensor/>
- ¹⁷ Spinning Sun Sensor. (n.d.). Retrieved from <http://www.adcole.com/aerospace/spinning-sun-sensors/spinning-sun-sensor/>
- ¹⁸ Solar tracking | Solar MEMS Sun Sensor. (n.d.). Retrieved from <http://www.solar-mems.com/solar-tracking/>



-
- ¹⁹ Northrop Grumman (2013). *LN-200S Inertial Measurement Unit (IMU)*[Brochure]. Woodland Hills, CA.
- ²⁰ ATA (2012). *Inertial Measurement Unit*[Brochure]. Albuquerque, NM.
- ²¹ Honeywell (2016). *HG1700 Inertial Measurement Unit*[Brochure]. Phoenix, AZ.
- ²² Near Earth Network (NEN) Users' Guide. 2018, Near Earth Network (NEN) Users' Guide.
- ²³ Wertz, J. R., Everett, D. F., & Puschell, J. J. (2015). *Space mission engineering: The new SMAD*. Hawthorne: Microcosm Press.
- ²⁴ SpaceX. *Falcon 9 Launch Vehicle Payload User's Guide*. SpaceX, 2015.
- ²⁵ Reshift Media. “7 Things to Consider When Choosing an Aluminum Grade | Metal Supermarkets.” *Metal Supermarkets*, 9 May 2016, www.metalsupermarkets.com/7-things-consider-choosing-aluminum-grade/.
- ²⁶ Edberg, Donald. *Introduction to Spacecraft Design and System Engineering*. University Readers, 2016.